Biophysical Journal
Article

Biophysical Society

Experimental Estimation of Membrane Tension Induced by Osmotic Pressure

Sayed Ul Alam Shibly,[1] Chiranjib Ghatak,[2] Mohammad Abu Sayem Karal,[1] Md. Moniruzzaman,[1] and Masahito Yamazaki[1,2,3,*]

[1]Integrated Bioscience Section, Graduate School of Science and Technology, [2]Nanomaterials Research Division, Research Institute of Electronics, and [3]Department of Physics, Faculty of Science, Shizuoka University, Shizuoka, Japan

ABSTRACT Osmotic pressure (Π) induces the stretching of plasma membranes of cells or lipid membranes of vesicles, which plays various roles in physiological functions. However, there have been no experimental estimations of the membrane tension of vesicles upon exposure to Π. In this report, we estimated experimentally the lateral tension of the membranes of giant unilamellar vesicles (GUVs) when they were transferred into a hypotonic solution. First, we investigated the effect of Π on the rate constant, k_p, of constant-tension (σ_{ex})-induced rupture of dioleoylphosphatidylcholine (DOPC)-GUVs using the method developed by us recently. We obtained the σ_{ex} dependence of k_p in GUVs under Π and by comparing this result with that in the absence of Π, we estimated the tension of the membrane due to Π at the swelling equilibrium, σ_{osm}^{eq}. Next, we measured the volume change of DOPC-GUVs under small Π. The experimentally obtained values of σ_{osm}^{eq} and the volume change agreed with their theoretical values within the limits of the experimental errors. Finally, we investigated the characteristics of the Π-induced pore formation in GUVs. The σ_{osm}^{eq} corresponding to the threshold Π at which pore formation is induced is similar to the threshold tension of the σ_{ex}-induced rupture. The time course of the radius change of GUVs in the Π-induced pore formation depends on the total membrane tension, σ_t; for small σ_t, the radius increased with time to an equilibrium one, which remained constant for a long time until pore formation, but for large σ_t, the radius increased with time and pore formation occurred before the swelling equilibrium was reached. Based on these results, we discussed the σ_{osm}^{eq} and the Π-induced pore formation in lipid membranes.

INTRODUCTION

When cells or vesicles of lipid membranes are transferred into a hypotonic solution containing a lower concentration of solute compared with the solution inside the cells or vesicles, an osmotic pressure, Π, is applied to the cells or vesicles. This results in water molecules entering the cells or vesicles, causing their volume to increase (the cells or vesicles swell). In turn, this induces a lateral tension in the plasma membrane or lipid membrane, and this tension plays various important roles in the physiological functions and physicochemical properties of the membrane (1–4). When the tension reaches a critical magnitude, pore formation occurs, causing lysis (rupture) of the vesicles which induces leakage (efflux) of their internal contents (5,6). The Π-induced increase of vesicle volume was used to investigate the elastic properties of lipid bilayers of large unilamellar vesicles (LUVs) by measuring the change of average diameters of the LUVs under Π using dynamic light scattering (DLS) (7–9). The Π-induced leakage of fluorescent probes was also measured and analyzed (5,10,11). However, all measurements to date of the effects of Π on vesicles have focused only on the Π-induced volume increase of vesicles (6–14) and the leakage of their internal contents. There have been no experimental estimations of the membrane tension of vesicles of lipid membranes upon exposure to Π. Moreover, all previous experiments have been conducted using LUVs. The polydispersity of LUVs (i.e., large distribution in LUV diameters) affects analysis by DLS (11), and fluorescence intensity measurements of LUV suspensions provide an ensemble average of the fluorescence intensity of many LUVs (15). In contrast, giant unilamellar vesicles (GUVs) of lipid membranes with diameters >10 μm have the advantage that their structures and physical properties can be directly observed as a function of time using optical microscopy (16–19). Measurement of the diameter and

Submitted August 16, 2016, and accepted for publication September 23, 2016.

*Correspondence: yamazaki.masahito@shizuoka.ac.jp

Mohammad Abu Sayem Karal's present address is Department of Physics, Bangladesh University of Engineering and Technology, Dhaka-1000, Bangladesh.

Editor: Ana-Suncana Smith.

http://dx.doi.org/10.1016/j.bpj.2016.09.043

observation of the shape of each GUV allows the selection of GUVs with a specific shape and an appropriate diameter for each experiment. Using this advantage, osmotic-pressure-induced shape changes of GUVs were observed (20,21). The shrinkage of a GUV after its transfer to a hypertonic environment was observed, and by analysis of the time course of the volume decrease of each GUV, the water permeability of lipid membranes was determined (22,23). The advantage of this approach was that the osmotic shrinkage of each GUV could be measured individually, and not as an ensemble average of many vesicles, as had been the case with previous measurements using LUVs.

It is well known that external forces also induce lateral tension on the plasma membranes of cells or the lipid membranes of vesicles, causing rupture of the cell or vesicle or pore formation in the membrane. There has been recent significant progress in research on tension-induced pore formation in lipid membranes using GUVs (16,24–29). Using a viscous solvent, Brochard-Wyart et al. visualized directly at video rate the fast dynamics of pore closing in a GUV stretched using intense optical illumination (16,24). Evans et al. investigated the rupture of a GUV under dynamic applied tension, in which ramps of tension with loading rates (i.e., tension/time) were applied using a micropipette (25,26). Recently, we developed a method to determine the rate constant of constant-tension (σ_{ex})-induced rupture of a GUV as a function of σ_{ex} using the concept of mean first passage time (MFPT) (27).

Understanding the effect of Π on the activities of membrane proteins and membrane active peptides such as antimicrobial peptides (19), and on the physicochemical properties of lipid membranes, requires information on the quantitative values of lateral tension due to Π. In this report, we estimated experimentally the lateral tension on the membranes of GUVs after transfer to a hypotonic solution. For this purpose, we followed a new idea. If we apply an external force to a GUV to induce a constant tension, σ_{ex}, in the presence of Π, the total tension, σ_t, on the GUV membrane is increased by the lateral tension due to Π, and thus, the rate constant of σ_{ex}-induced rupture of a GUV, k_p, increases. Therefore, if we compare the σ_{ex} dependence of k_p in GUVs under Π with that in the absence of Π (27) to obtain the difference of the values of σ_{ex} to induce the same k_p value, we can estimate the membrane tension due to Π. Based on this idea, we made several kinds of experiments. First, we investigated the effect of Π on the k_p of σ_{ex}-induced rupture in GUVs composed of dioleoylphosphatidylcholine (DOPC) using the method developed by us recently (27). By obtaining the σ_{ex} dependence of k_p in GUVs under Π and comparing this result with that obtained in the absence of Π, we estimated the membrane tension of the GUVs at swelling equilibrium under Π, σ_{osm}^{eq}. Next, we measured the volume change of DOPC-GUVs under small Π. The experimentally obtained values of σ_{osm}^{eq} and the volume change were compared with the theoretical values. Finally, we investigated Π-induced pore formation in GUVs and compared this result with that of σ_{ex}-induced rupture.

MATERIALS AND METHODS

Preparation and observation of DOPC-GUVs

DOPC was purchased from Avanti Polar Lipids (Alabaster, AL). 6-Dodecanoyl-2- (dimethylamino)-naphthalene (Laurdan) was purchased from Invitrogen (Carlsbad, CA). Bovine serum albumin (BSA) was purchased from Wako Pure Chemical Industry Ltd. (Osaka, Japan). DOPC-GUVs were prepared by natural swelling in water (MilliQ) containing sucrose as follows (27). DOPC in chloroform (1.0 mM, 200 μL) in a small glass bottle (5 mL) was dried by N_2 gas to produce a thin, homogeneous lipid film; then, residual chloroform in the film was removed by placing the bottle in a vacuum desiccator connected to a rotary vacuum pump for >12 h. MilliQ water (20 μL) was added and the bottle was sealed and incubated in 45–47°C water for 8 min (prehydration). Then, 1.0 mL of 100.0 mM sucrose in MilliQ was added gently, and the bottle was resealed and incubated in an incubator at 37°C for 2 h to produce a GUV suspension. The GUV suspension (20 μL, 98.0 mM sucrose aqueous solution) was diluted into 280 μL of various concentrations of glucose aqueous solution, and each mixture was transferred into a hand-made chamber (15). The GUVs were observed using an inverted fluorescence phase-contrast and differential interference contrast (DIC) microscope (IX-71, Olympus, Tokyo, Japan) at 25 $\pm$ 1°C using a stage thermocontrol system (Thermoplate, Tokai Hit, Shizuoka, Japan). Phase-contrast and DIC images of GUVs were recorded using a CCD camera (CS230B, Olympus) with a hard disk.

All experiments described below used DOPC-GUVs within 2 h of their preparation (i.e., after the incubation at 37°C) to increase the reproducibility of the data and the GUVs were placed and used in the chamber within 30 min of being transferred to the glucose solution to prevent any effect of water evaporation from the chamber.

Measurement of the rate constant of constant-tension-induced rupture of a GUV under Π

We used our recently developed method to measure the rate constant of the σ_{ex}-induced rupture of a GUV (27). To apply Π on a GUV, first the GUV suspension was transferred into a chamber containing a lower concentration of glucose solution in MilliQ water compared to the solution inside the GUV. Swelling equilibrium was attained after >5 min incubation, then external tension was applied to a single GUV using a glass micropipette prepared by pulling a 1.0 mm glass capillary composed of borosilicate glass (G-1, Narishige, Tokyo, Japan) using a puller (PP-83 or PC-10, Narishige, Tokyo, Japan) (15). A single GUV was held for 2 min at the tip of a micropipette containing the same concentration of glucose solution as in the chamber by applying slight suction pressure (i.e., the difference in pressure between the outside and the inside of a micropipette, ΔP_m), thus providing a tension of 0.5 mN/m on the bilayer. The GUV was then rapidly (in ~10 s) aspirated to apply a specific tension on the GUV membrane, and this tension remained constant until the GUV was completely aspirated into the micropipette as a result of rupture of the GUV, or after 6 min, whichever occurred first. The time of rupture was defined as the time when the GUV was completely aspirated and was measured with a time resolution of <1 s. The σ_{ex} of the GUV membrane due to an external force produced by the suction pressure can be described as a function of ΔP_m as follows (17):

$$\sigma_{ex} = \frac{\Delta P_m d_P}{4(1 - d_P/D_V)}, \quad (1)$$

where d_p is the internal diameter of the micropipette and D_v is the diameter of the spherical part of the GUV outside the micropipette. Micropipettes with d_p = 7.0–8.0 μm were used. The micropipettes were coated with 0.5% (w/v) BSA in glucose solution and the glass surfaces in the chambers were coated with 0.1% (w/v) BSA in glucose solution; in all cases, excess BSA solution was removed by washing using glucose solution, leaving a BSA coating on the glass surfaces (15,27–29). ΔP_m was measured using a differential pressure transducer (DP15, Validyne, Northridge, CA), pressure amplifier (PA501, Validyne), and a digital multimeter (15).

Measurement of Π-induced volume changes of DOPC-GUVs

Here, we applied the similar method used to measure the volume decrease of a GUV upon transfer into a hypertonic solution (23,30). To apply Π to a GUV held at the tip of a micropipette, the GUV was transferred from a chamber (chamber A) containing 98.0 mM glucose in MilliQ water, and thus isotonic against the 98.0 mM sucrose solution inside the GUV, to another chamber (chamber B) containing a lower concentration of glucose solution in MilliQ water that was thus hypotonic against the solution inside the GUV. A single GUV in chamber A was held by a micropipette using a tension of 0.5 mN/m for 2 min and then transferred into chamber B, which contained glucose solution with a lower osmolarity. To circumvent the small air gap between the two chambers, we used a glass capillary with a diameter of 1.0 mm filled with 98.0 mM glucose solution to transfer the GUV from chamber A to chamber B. After the transfer, the glass capillary was retracted from the GUV, and then the concentration of glucose solution in the vicinity of the GUV was rapidly changed to that of the bulk solution in chamber B. The volume change of the GUV, ΔV, was determined by the change in the projection length of the GUV inside the micropipette, ΔL, as follows (23):

$$\Delta V = V - V_0 \approx -\pi d_P \left(D_V - d_p\right) \Delta L / 4, \tag{2}$$

where V and V_0 are the volume of the GUV at $t = t$ and $t = 0$, respectively (t is the time after the transfer of the GUV into chamber B). For the experiments described in Time Course of the Radius Change of DOPC-GUVs Induced by Π, membrane tensions >0.5 mN/m (4.0−5.0 mN/m) were applied by micropipette aspiration, whereas all other experimental procedures were as described above.

Measurement of Π-induced leakage of the internal content from DOPC-GUVs

Π was applied on a GUV using the method described in Measurement of Π-Induced Volume Changes of DOPC-GUVs. After transfer of the GUV from chamber A to chamber B, we decreased the suction pressure and released the GUV into the hypotonic solution in the chamber. The GUV sank gradually to the bottom of the chamber. We continuously observed the moving GUV by keeping it in focus under the microscope, and recorded the images of the GUV at video rate (i.e., 1 frame/33 ms).

Theory on the membrane tension of a GUV induced by Π

Here we consider the response of a GUV under Π. Before the application of Π, a GUV has an initial radius of r_0, its initial surface area and initial volume are A_0 and V_0, respectively, and the initial sucrose concentration inside the GUV is ${C_{in}}^0$. When we transfer the GUV into a hypotonic solution where the glucose concentration is C_{out} ($< {C_{in}}^0$) (i.e., $\Delta C^0 = {C_{in}}^0 - C_{out}$) (where the units of all the concentrations are mol/m^3 (mM)), Π is applied to the GUV due to the difference in the chemical potential of water inside and outside of the GUV. It is reported that when the concentrations, C, of sucrose and glucose are low (i.e., $C < 100$ mM) the linearity between Π and C holds, and thus, the ideal equation (van't Hoff's law) for Π can be used (31,32). We also measured osmolarity (mOsm/L) of sucrose and glucose solutions of <98 mM and obtained the linear relationship between the osmolarity and the molar concentration (Fig. S1 in the Supporting Material). Therefore, here we can use $\Pi = RT\Delta C^0$, where R is the gas constant and T is the absolute temperature. Due to Π, water molecules start to enter the GUV and the radius and the volume of the GUV increase, inducing an increase in the surface area of the GUV, which creates a lateral tension, σ_{osm}, in the GUV membrane produced by its stretching. This produces the hydrostatic pressure difference between the inside and the outside of the GUV, ΔP ($= P_{in} - P_{out}$). The volume increase also induces a decrease in sucrose concentration inside the GUV. When the radius of the GUV increases by Δr (i.e., its radius is $r_0 + \Delta r$, and its surface area and its volume are $A_0 + \Delta A$ and $V_0 + \Delta V$, respectively), $\Delta P(\Delta r)$ can be expressed by the following equation using the Laplace law (33):

$$\Delta P(\Delta r) = \frac{2\sigma_{osm}(\Delta r)}{r_0 + \Delta r}. \tag{3}$$

It is noted that σ_{osm} is a function of Δr, i.e., $\sigma_{osm}(\Delta r)$. Π also decreases due to the dilution of the sucrose concentration inside the GUV until it reaches $\Pi(\Delta r)$. If $\Pi(\Delta r) > \Delta P(\Delta r)$, water molecules continue to enter the GUV. When the swelling of the GUV reaches equilibrium, Δr, ΔA, and ΔV attain their equilibrium values, Δr_{eq}, ΔA_{eq}, and ΔV_{eq}, respectively, and $\Delta P^{eq} = \Pi^{eq} = RT\Delta C^{eq}$, where $\Delta C^{eq} = C_{in}^{eq} - C_{out}$ (here, ${C_{in}}^{eq}$ is C_{in} at swelling equilibrium) and $\sigma_{osm}(\Delta r)$ reaches its equilibrium value, σ_{osm}^{eq}. Therefore, we can obtain σ_{osm}^{eq} from ΔC^{eq} as follows:

$$\sigma_{osm}^{eq} = \frac{RT\left(r_0 + \Delta r_{eq}\right)}{2}\Delta C^{eq}, \tag{4}$$

where

$$\begin{aligned}\Delta C^{eq} = C_{in}^{eq} - C_{out} &= \left\{\frac{C_{in}^0 V_0}{V_0 + \Delta V_{eq}} - C_{out}\right\} \\ &\approx \left\{\frac{C_{in}^0}{1 + 3\left(\Delta r_{eq}/r_0\right)} - C_{out}\right\}\end{aligned} \tag{5}$$

We used an approximation for $\Delta V_{eq}/V_0 \approx 3(\Delta r_{eq}/r_0)$, because the GUV is spherical and Δr_{eq} is very small. On the other hand, we can obtain σ_{osm}^{eq} using the elastic modulus of the bilayer of the GUV, K_{bil}, as follows (17):

$$\sigma_{osm}^{eq} = K_{bil}\frac{\Delta A_{eq}}{A_0} \approx 2K_{bil}\frac{\Delta r_{eq}}{r_0}. \tag{6}$$

Similarly, here we used an approximation for $\Delta A_{eq}/A_0 \approx 2(\Delta r_{eq}/r_0)$, because the GUV is spherical and Δr_{eq} is very small. From Eqs. 4–6, we obtained an equation to derive $\Delta r_{eq}/r_0$ as follows:

$$\frac{\Delta r_{eq}}{r_0} = \frac{RT\Delta C^0/2}{\frac{2K_{bil}}{r_0} + \frac{3RTC_{out}}{2} - \frac{RT\Delta C^0}{2}}, \tag{7}$$

where higher-order terms of $(\Delta r_{eq}/r_0)^n$ with $n \geq 2$ were neglected. The first term of the denominator in Eq. 7 represents the dependence of $\Delta r_{eq}/r_0$ on K_{bil} and r_0. From Eqs. 6 and 7, we can obtain σ_{osm}^{eq}. We measured the value of K_{bil} of a DOPC-GUV in 100 mM sucrose (inside the GUV)/100 mM glucose (outside the GUV) using the standard method (34,35), and obtained its mean value and the standard deviation; $K_{bil} = 218 \pm 26$ mN/m ($n = 16$)

(Fig. S2), which is almost the same as reported values (17,35). We consider the example where C_{in}^{0} = 98.0 mM, C_{out} = 96.0 mM (hence, ΔC^0 = 2.0 mM), r_0 = 10.0 μm, K_{bil} = 218 mN/m, and T = 298 K. From Eq. 7, we obtain $\Delta r_{eq}/r_0 = 6.2 \times 10^{-3}$. Using Eq. 6, σ_{osm}^{eq} = 2.7 mN/m. Using Eq. 5, $\Delta C^{eq} = C_{in}^{eq} - C_{out}$ = 98.2−98.0 = 0.2 mM. In this case, each term of the right side of Eq. 7 is as follows; 2500 Pa for the numerator, 44,000 Pa for the first term of the denominator, 360,000 Pa for the second term, and 2,500 for the third term. In most experiments done in this study, we used ΔC^0 values in the range of 1.0 – 8.0 mM, which correspond to $\sigma_{osm}^{eq} = (1.4 \sim 1.5)\Delta C_0$ (mN/m) (Table S4).

RESULTS AND DISCUSSION

Effect of Π on constant-tension-induced rupture in DOPC-GUVs

We investigated the effect of Π on the constant-tension-induced rupture of single DOPC-GUVs. First, we examined the effect of Π due to the initial difference in solute concentration between the inside and the outside of the GUV, ΔC^0 (i.e., 2.8 mM). The external, constant tension, σ_{ex}, of the GUV membrane due to aspiration was 3.8 mN/m. For this purpose, we first transferred GUVs containing 98.0 mM sucrose solution into a chamber containing 95.0 mM glucose solution (final solute concentration outside the GUVs were 95.2 mM) and incubated the suspension for >5 min so that the swelling of the GUV attained equilibrium against Π. Next, a single GUV was held at the tip of a micropipette for 2 min using only slight aspiration pressure to provide a tension of 0.5 mN/m on the bilayer to eliminate the problems of the hidden area (17,27). Then the GUV was rapidly (in ~10 s) aspirated to obtain a tension of 3.8 mN/m (Fig. 1 *A*). After a period of time, the GUV was suddenly aspirated into the micropipette. Based on our previous articles (27,28), this sudden aspiration is due to a pore forming in the GUV membrane, causing rupture of the GUV and complete aspiration of the GUV into the micropipette due to the pressure difference between the inside and the outside of the micropipette. When we repeated the same experiment with 19 single GUVs (n = 19), we found that rupture of a GUV occurred stochastically at different times. The time course of the fraction of intact (unruptured) GUVs among all the GUVs, P_{intact} (t) (27), was fit to a single exponential decay function as follows (Fig. 1 *B*, *open squares*).

$$P_{intact}(t) = \exp(-k_p t), \quad (8)$$

where k_p is the rate constant of σ_{ex}-induced rupture formation, which is the same as the rate constant of σ_{ex}-induced pore formation, and t represents the duration of the tension applied to the GUV. This fitting provided a k_p value of 6.9×10^{-3} s^{-1}. Next, the same experiment was performed using 4.3 mN/m (n = 19). P_{intact} (t) decreased more rapidly with time (Fig. 1 *B*, *open circles*), and curve fitting provided a k_p value of 2.5×10^{-2} s^{-1}. To obtain the σ_{ex} dependence of k_p, we conducted three independent experiments, each using 18−22 GUVs, and obtained mean values and standard errors for k_p. Fig. 1 *C* (*solid rhombus*) shows that the k_p of DOPC-GUVs for ΔC^0 = 2.8 mM increased with σ_{ex}. Next, we investigated the effect of Π for ΔC^0 = 1.9 mM (using a glucose concentration of 96.0 mM in the chamber, and final solute concentration outside the GUVs was 96.1 mM) on the σ_{ex}-induced rupture of a DOPC-GUV. Fig. 1 *C* (*solid triangle*) shows that the k_p value increased with σ_{ex}. For comparison, the experimental data for k_p of DOPC-GUVs without Π (ΔC^0 = 0.0 mM) (27) is also shown in Fig. 1 *C* (*open squares*). Fig. 1 *C* indicates that as ΔC^0 increased, lower tensions were required to produce the same values of k_p. In other words, the application of Π to DOPC-GUVs greatly increased the k_p of the GUV.

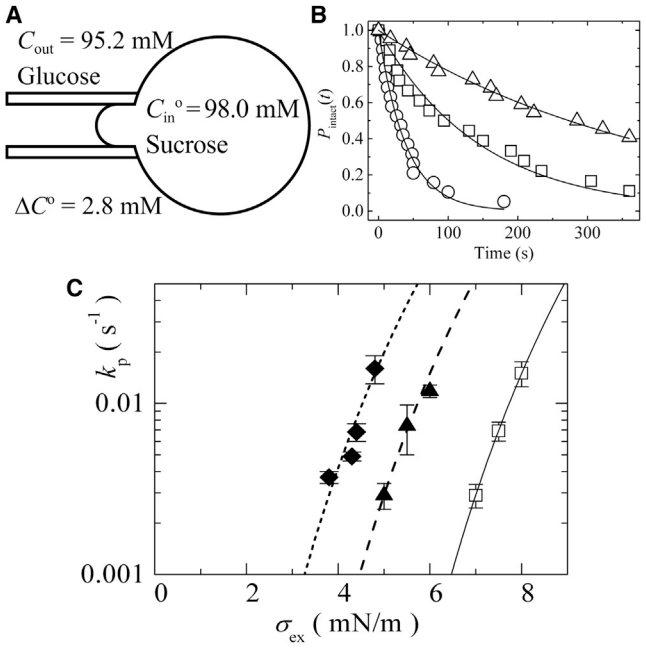

FIGURE 1 Effect of Π on constant-tension-induced rupture of DOPC-GUVs. (*A*) A scheme of the measurement for $\Delta C^0 = C_{in}^{0} - C_{out}$ = 2.8 mM, where C_{in}^{0} is the initial sucrose concentration inside a GUV and C_{out} is the glucose concentration on the outside of the GUV. (*B*) Time course of the fraction of intact DOPC-GUVs without rupture among all of the examined GUVs, $P_{intact}(t)$, in the presence of Π due to ΔC^0 = 2.8 mM and tension due to the micropipette aspiration: σ_{ex} = 3.3 mN/m (*open triangles*), 3.8 mN/m (*open squares*), and 4.3 mN/m (*open circles*). The number of single GUVs examined was 18−22 in each experiment. The solid lines represent the best-fit curves of Eq. 8. (*C*) Dependence of k_p on external tension for ΔC^0 = 1.9 mM (*solid triangle*), ΔC^0 = 2.8 mM (*solid rhombus*), and ΔC^0 = 0 mM (*open squares*) (i.e., no osmotic pressure). Error bars show standard errors. The solid lines show the best fits in accordance with the theoretical curves corresponding to Eq. 9 using Γ = 10.5 pN and D_r = 165 nm^2/s. The data for ΔC^0 = 0.0 mM (*open squares*) and its fitting curve are reprinted from (27) with permission from the American Chemical Society. The dashed line and the dotted line correspond to the theoretical Eq. 9 using $\sigma_t = \sigma_{ex}$ + 2.6 mN/m and $\sigma_t = \sigma_{ex}$ + 3.8 mN/m, respectively.

Here, we experimentally estimated the membrane tension due to Π at swelling equilibrium, σ_{osm}^{eq}, by analyzing the results of Fig. 1 *C*. We can reasonably assume the additivity of the tension σ_{ex} due to aspiration according to eq. 1 and the

tension due to Π, σ_{osm}^{eq}, according to eq. 6, and hence the total tension, σ_t, can be expressed by $\sigma_t = \sigma_{ex} + \sigma_{osm}^{eq}$. Moreover, the value of k_p is determined by σ_t. When we compare σ_{ex} values which induce the same values of k_p under different conditions (Fig. 1 *C*), the difference between σ_{ex} of the GUV in the presence of Π and σ_{ex} of the GUV without Π corresponds to σ_{osm}^{eq} of the GUV in the presence of Π. The values of σ_t of the GUV without Π for specific values of k_p were determined by the following theoretical equation, which fits well to the experimental results of k_p versus σ_t (27):

$$k_p = \frac{\sqrt{3}D_r\sigma_t}{kT}\exp\left(-\frac{\pi\Gamma^2}{kT\sigma_t}\right), \quad (9)$$

where D_r is the diffusion coefficient of a particle in *r*-phase space, Γ is the line energy per unit length of a prepore rim in lipid bilayers (i.e., the line tension), and *k* is the Boltzmann constant. Here, we assumed a hydrophilic prepore and obtained the values of the parameters for the DOPC membrane by analysis of the relationship between k_p and σ_t using Eq. 9: $\Gamma = 10.5$ pN and $D_r = 165$ nm^2/s (27). For the value of Γ for the hydrophilic pore, Karatekin et al. obtained 6.9 – 20.7 pN depending on the provider of DOPC, as determined by analysis of the closure dynamics of transient pores (24). However, here we used $\Gamma = 10.5$ pN because it was obtained by the best-fitting data according to Eq. 9. Next, we explain an example of the analysis using Eq. 9. For $\Delta C^0 = 1.9$ mM, $k_p = 1.7 \times 10^{-2}$ s^{-1} at $\sigma_{ex} = 5.5$ mN/m (experimental data), and σ_{ex} in the absence of Π (i.e., $\Delta C^0 = 0$ mM), which induced the same k_p value (i.e., 1.7×10^{-2} s^{-1}), was 8.1 mN/m according to Eq. 9. Hence, the difference between σ_{ex} ($\Delta C^0 = 0$ mM) and σ_{ex} ($\Delta C^0 = 1.9$ mM) is 2.6 mN/m, which corresponds to the experimentally determined σ_{osm}^{eq}, $(\sigma_{osm}^{eq})^{ex}$, for this condition. We also calculated $(\sigma_{osm}^{eq})^{ex}$ for other conditions, such as k_p and ΔC^0 (Tables 1 and 2). The mean values of $(\sigma_{osm}^{eq})^{ex}$ for different σ_{ex} values were 2.6 ± 0.1 mN/m for $\Delta C^0 = 1.9$ mM and 3.8 ± 0.1 mN/m for $\Delta C^0 = 2.8$ mM. Therefore, for $\Delta C^0 = 1.9$ mM, $\sigma_t = \sigma_{ex} + 2.6$ mN/m. Using this value of σ_t and the same values of Γ and D_r as in the absence of Π, we plotted the theoretical curve (Eq. 9) of k_p versus σ_t in Fig. 1 *C* (*dashed line*). Similarly, for $\Delta C^0 = 2.8$ mM, $\sigma_t = \sigma_{ex} + 3.8$ mN/m, and using this value of σ_t we plotted the theoretical curve of k_p versus σ_t in Fig. 1 *C* (*dotted line*). Both theoretical curves fit well to the experimental results. To our knowledge, these data provide the first experimentally determined membrane tensions induced by Π.

On the other hand, using the theory described in Theory on the Membrane Tension of a GUV Induced by Π, we determined the theoretical values of σ_{osm}^{eq}, $(\sigma_{osm}^{eq})^{th}$: 2.6 ± 0.7 mN/m for $\Delta C^0 = 1.9$ mM, and 3.9 ± 0.7 mN/m for $\Delta C^0 = 2.8$ mM. Here, we estimated the error of $(\sigma_{osm}^{eq})^{th}$ from the errors of ΔC^0, C_{out}, and K_{bil}. The errors of ΔC^0 and C_{out} were evaluated based on the method of preparation of the sucrose and glucose solutions: the errors of these concentrations are estimated to be ±0.2 mM for the 100 mM sucrose solution and ±0.5 mM for the 100 mM glucose solution, and hence, the error of ΔC^0 is ±0.5 mM. The variation of the initial radius of a GUV, r_0, does not affect the value of $(\sigma_{osm}^{eq})^{th}$ significantly. For the experiments at $\Delta C^0 = 1.9$ mM, we calculated $(\sigma_{osm}^{eq})^{th}$ for various sizes of GUVs under the same conditions: 2.7 mN/m for $r_0 = 20$ μm and 2.6 mN/m for $r_0 = 10$ μm. Therefore, we conclude that the values of $(\sigma_{osm}^{eq})^{ex}$ agree with those of $(\sigma_{osm}^{eq})^{th}$ within the limits of the experimental errors, indicating that the theory described in Materials and Methods (Theory on the Membrane Tension of a GUV Induced by Π) is correct.

Increase in the volume of DOPC-GUVs induced by Π

According to the above-referenced theory, if we can determine Π-induced Δr_{eq} experimentally, we can estimate σ_{osm}^{eq} indirectly. For this purpose, we measured the volume change of a single DOPC-GUV upon exposure to Π using the method developed by Evans and colleagues (23). A single GUV containing 98.0 mM sucrose solution was held at the tip of a micropipette for a few minutes using only slight aspiration pressure in chamber A, which contained 98.0 mM glucose solution (the tension applied to the bilayer was 0.5 mN/m). The GUV was then transferred to chamber B, which contained 96.0 mM glucose solution (i.e., $\Delta C^0 = 2.0$ mM). The projection length, Δ*L*, of the GUV inside the micropipette (Fig. 2 *A*) decreased with time and attained an equilibrium value, ΔL_{eq}, after 70 s. Using Eq. 2, we calculated the volume change of the GUV, Δ*V*, to obtain the ratio of Δ*V* to its initial volume, V_0, i.e., $\Delta V/V_0$. Fig. 2 *B* (*solid circles*) indicates that $\Delta V/V_0$ increased with time to an equilibrium value, $\Delta V_{eq}/V_0$. The mean value of

TABLE 1 Comparison of the External Tensions that Induced the Same k_p Values in the Presence and Absence of Osmotic Pressure

σ_{ex} (mN/m) with ΔC^0	k_p (s^{-1})	σ_{ex} (mN/m) with $\Delta C^0 = 0$[a]	σ_{osm}^{eq} (mN/m) = σ_{ex} ($\Delta C^0 = 0$) − σ_{ex} (ΔC^0)	$\overline{(\sigma_{osm}^{eq})^{ex}}$ (mN/m)	$(\sigma_{osm}^{eq})^{th}$ (mN/m)	$\overline{r_0}$ (μm)
4.5	3.2×10^{-3}	7.1	2.6	2.6 ± 0.1	2.6 ± 0.7	13.4 ± 0.2
5.0	9.4×10^{-3}	7.7	2.7			
5.5	1.7×10^{-2}	8.1	2.6			

Values are from the analysis of the data for $\Delta C^0 = 1.9$ mM in Fig. 1. $\overline{(\sigma_{osm}^{eq})^{ex}}$ and $\overline{r_0}$ are mean values of $(\sigma_{osm}^{eq})^{ex}$ and r_0, respectively.
[a]Values were obtained using Eq. 9.

TABLE 2 Comparison of the External Tensions that Induced the Same k_p Values in the Presence and Absence of Osmotic Pressure

σ_{ex} (mN/m) with ΔC^0	k_p (s^{-1})	σ_{ex} (mN/m) with $\Delta C^0 = 0$[a]	σ^{eq}_{osm} (mN/m) = σ_{ex} ($\Delta C^0 = 0$) − σ_{ex} (ΔC^0)	$\overline{(\sigma^{eq}_{osm})^{ex}}$ (mN/m)	$(\sigma^{eq}_{osm})^{th}$ (mN/m)	$\overline{r_0}$ (μm)
3.3	3.5×10^{-3}	7.1	3.8	3.8 ± 0.1	3.9 ± 0.7	13.7 ± 0.2
3.8	9.3×10^{-3}	7.7	3.9			
4.3	1.5×10^{-2}	8.0	3.7			

Values are from the analysis of the data for $\Delta C^0 = 2.8$ mM in Fig. 1. $\overline{(\sigma^{eq}_{osm})^{ex}}$ and $\overline{r_0}$ are mean values of $(\sigma^{eq}_{osm})^{ex}$ and r_0, respectively.
[a]Values were obtained using Eq. 9.

$\Delta V_{eq}/V_0$ was $(1.7 \pm 0.1) \times 10^{-2}$ ($n = 14$). The same experiments were performed using $\Delta C^0 = 3.0$ mM (Fig. 2 *B*, *open squares*); the time course of $\Delta V/V_0$ was similar to that for $\Delta C^0 = 2.0$ mM, and $\Delta V_{eq}/V_0 = (2.6 \pm 0.1) \times 10^{-2}$ ($n = 17$). In the control experiment ($\Delta C^0 = 0.0$ mM) (Fig. 2 *B*, *open circles*), no significant change in $\Delta V/V_0$ was observed for 20 min after transfer to chamber B.

As shown in Fig. 2 *B*, $\Delta V_{eq}/V_0$ increased with ΔC^0. This result indicates that higher Π induces larger swelling of GUVs, which can be reasonably explained by Eq. 7. Moreover, the values of $\Delta V_{eq}/V_0$ allow us to experimentally estimate the membrane tension due to Π at swelling equilibrium of the GUV, $(\sigma^{eq}_{osm})^{ex}$. Since Δr is small, $(\Delta r_{eq}/r_0) \approx (1/3)\Delta V_{eq}/V_0 = (5.6 \pm 0.1) \times 10^{-3}$. Using Eq. 6, $(\sigma^{eq}_{osm})^{ex} = 2.7 \pm 0.1$ mN/m. We can also obtain the values of $(\sigma^{eq}_{osm})^{th}$ using the above-referenced theory. For $\Delta C^0 = 2.0 \pm 0.5$ mM, we obtained $\Delta r_{eq}/r_0 = (6.4 \pm 1.6) \times 10^{-3}$ using Eq. 7, and hence $(\sigma^{eq}_{osm})^{th} = 2.8 \pm 0.7$ mN/m using Eq. 6 (Table S3). For $\Delta C^0 = 3.0$ mM, $(\sigma^{eq}_{osm})^{ex} = 4.1 \pm 0.2$ mN/m, since $(\Delta r_{eq}/r_0) = (8.6 \pm 0.2) \times 10^{-3}$. On the other hand, theoretically, $\Delta r_{eq}/r_0 = (9.8 \pm 1.7) \times 10^{-3}$ and $(\sigma^{eq}_{osm})^{th} = 4.3 \pm 0.7$ mN/m (Table S3). The dependence of the theoretical values of $\Delta V_{eq}/V_0$ obtained by Eq. 6 on r_0 is very small, and therefore, the experimental values of σ^{eq}_{osm} and $\Delta r_{eq}/r_0$ agree with the theoretical values within the limits of the experimental errors.

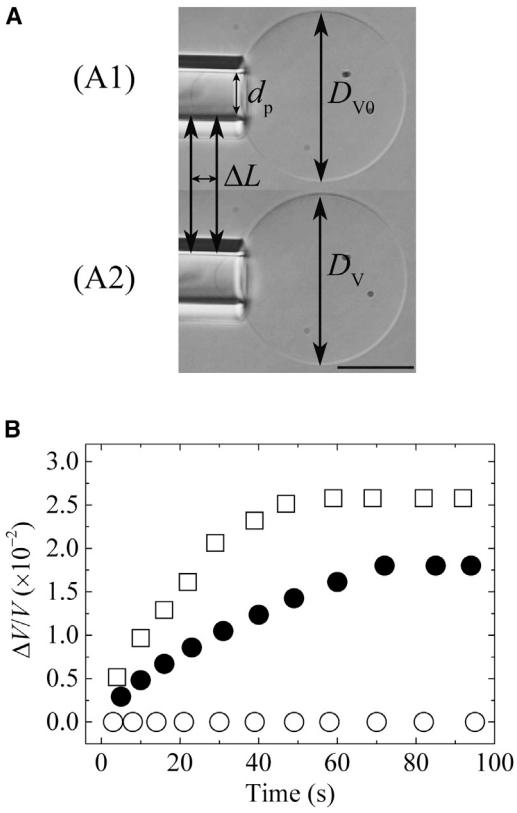

FIGURE 2 Increase in volume of DOPC-GUV induced by Π. (*A1*) A DIC image of a GUV held at the tip of a micropipette using a small aspiration pressure in chamber A, which contained an isotonic solution. (*A2*) A DIC image of a GUV held at the tip of a micropipette after the GUV was transferred into another chamber, chamber B, containing a hypotonic solution. d_p is the internal diameter of the micropipette and ΔL is the change of the projection length. The bar corresponds to 10 μm. (*B*) Time course of volume change of a GUV after it was transferred into chamber B, which contained 96.0 mM (i.e., $\Delta C^0 = 2.0$ mM; *solid circles*), 95.0 mM (i.e., $\Delta C^0 = 3.0$ mM; *open squares*), and 98.0 mM (i.e., $\Delta C^0 = 0.0$ mM, *open circles*) glucose solutions.

Rapid, transient leakage of sucrose from DOPC-GUVs induced by Π

Next, we investigated Π-induced pore formation in a GUV to compare it with the constant-tension-induced pore formation where the tension in the GUV membrane is produced by an external force (27). For this purpose, we initially held a single GUV containing 98.0 mM sucrose solution in chamber A, which contained 98.0 mM glucose solution, at the tip of a micropipette for a few minutes using only slight aspiration pressure. The tension on the bilayer was 0.5 mN/m. The GUV was then transferred into chamber B, which contained 90.0 mM glucose solution ($\Delta C^0 = 8.0$ mM), the suction pressure was decreased, and the GUV was released into the hypotonic solution in chamber B. The GUV was continuously observed after release. Fig. 3 *A* shows phase-contrast images of the response of a GUV in chamber A: the diameter of the GUV in chamber B at 31.033 s after transfer into chamber B was larger than its diameter in chamber A in the absence of Π. Rapid leakage of sucrose solution was observed at 31.066 ± 0.033 s (Fig. 3 *A*, *black arrow*), and consequently, the diameter of the GUV rapidly decreased in 33 ms (i.e., from 31.033 s to 31.066 s in Fig. 3 *A*); then, after 31.099 s, it gradually increased, indicating that the leakage of sucrose stopped at 31.099 ± 0.033 s. The phase contrast of the GUV did not decrease significantly due to this leakage. These results can be

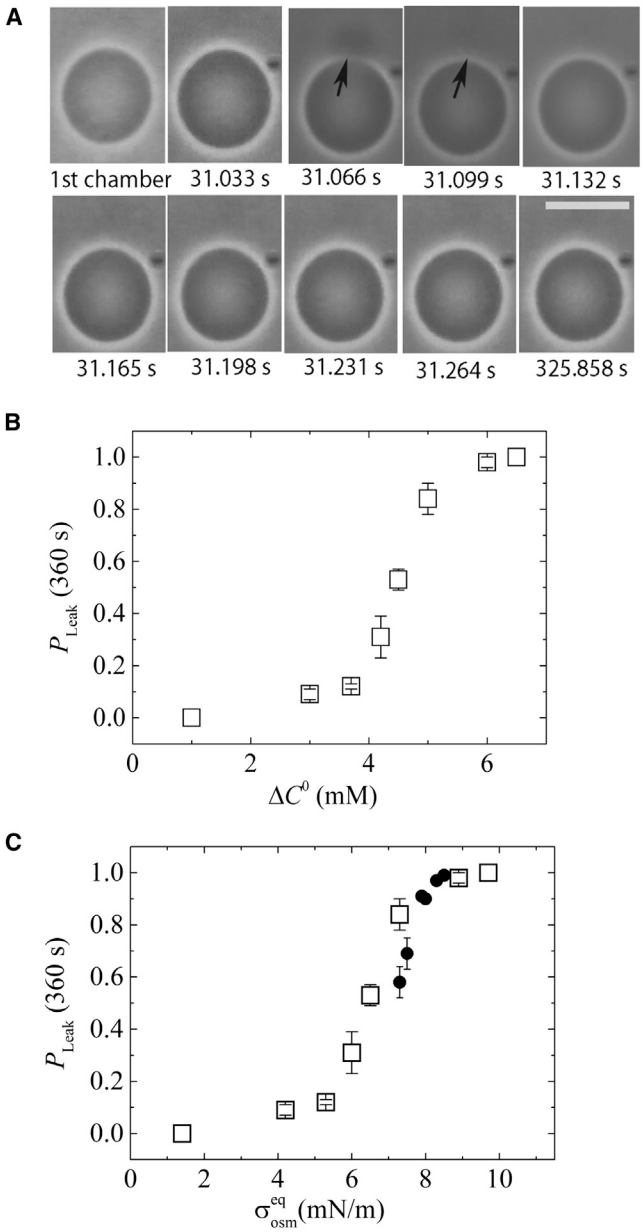

FIGURE 3 Large Π-induced pore formation in DOPC-GUVs. (*A*) Phase-contrast microscopic images of a GUV after it was transferred into chamber B, which contained 90.0 mM glucose solution (i.e., $\Delta C^0 = 8.0$ mM). The numbers below each image show the time in seconds after the transfer of the GUV into chamber B. Scale bar, 25 μm. The arrows show a rapid, transient leakage of sucrose from the DOPC-GUV. (*B*) The fraction of GUV where a transient leakage occurred during the first 6 min, P_{Leak} (360 s), as a function of ΔC^0. Mean values and standard errors of P_{Leak} (360 s) for each ΔC^0 were determined among three independent experiments using 10−15 GUVs for each experiment. Error bars show standard errors. (*C*) P_{Leak} (360 s) as a function of membrane tension due to Π at equilibrium, $\sigma^{eq}_{osm} = \sigma_t$ (*open squares*). ΔC^0 values in (*B*) were converted into σ^{eq}_{osm}. For comparison, the data in Fig. 1 were added (*solid circles*); the values of the fraction of ruptured GUVs during the first 6 min among all the examined GUVs, P_{pore} (360 s), were obtained for the theoretical values of $\sigma_t = \sigma_{ex} + \sigma^{eq}_{osm}$ for each condition of the experiments of Fig. 1.

considered as follows. First, sudden pore formation occurred in the GUV membrane due to the swelling of GUVs due to Π, inducing a transient leakage of a small amount of sucrose solution. Thus, the diameter of the GUV rapidly decreased, and then the leakage stopped within 99 ms after pore formation, indicating the resealing of the GUV membrane. Then, the GUV volume increased again due to Π. The time required for closure of the pore (here 99 ms) was determined by observation of visible sucrose leakage, and hence it is not accurate. This experiment was repeated using 21 GUVs and similar results were obtained.

We investigated the effect of ΔC^0 on the rate of Π-induced pore formation in lipid membranes. For the experiments shown in Fig. 3 *A*, we cannot obtain the rate constant of Π-induced pore formation, which is different from the σ_{ex}-induced rupture of GUVs (see Effect of Π on Constant-Tension-Induced Rupture in DOPC-GUVs). However, we can use one measure of this rate, namely, the fraction of GUVs in which transient leakage occurred during the first 6 min among all the examined GUVs, P_{Leak} (360 s) (27). Fig. 3 *B* shows that P_{Leak} (360 s) was negligible ($\leq$0.12) at $\Delta C^0 \leq 3.7$ mM, but at $\Delta C^0 \geq 4.2$ mM, P_{Leak} (360 s) increased with increasing ΔC^0 and reached 1.0 at $\Delta C^0 =$ 6.5 mM. This result indicates that the rate of Π-induced pore formation increased with an increase in ΔC^0, i.e., Π. After conversion of ΔC^0 to $(\sigma^{eq}_{osm})^{th}$ using Eqs. 6 and 7, we obtained the dependence of P_{Leak} (360 s) on $(\sigma^{eq}_{osm})^{th}$ (Fig. 3 *C*; Table S4). At $(\sigma^{eq}_{osm})^{th} \leq 5.3$ mN/m, P_{Leak} (360 s) was negligible ($\leq$0.12). At $(\sigma^{eq}_{osm})^{th} = 6.0$ mN/m, P_{Leak} (360 s) became significant ($= 0.31 \pm 0.08$), and at $(\sigma^{eq}_{osm})^{th} \geq 6.0$ mN/m, P_{Leak} (360 s) increased with $(\sigma^{eq}_{osm})^{th}$. This behavior is similar to the σ_{ex}-induced rupture of DOPC-GUVs (27).

We observed two transient leakages from most GUVs within 6 min for higher ΔC^0, such as $\Delta C^0 = 20$ mM (Fig. S3).

Time course of radius change of DOPC-GUVs induced by Π

In the previous section, we could not obtain accurate values for $\Delta r/r_0$ when pore formation occurred in a DOPC-GUV upon exposure to large Π, and therefore we applied the method used in Increase in the Volume of DOPC-GUVs Induced by Π. The first experiment used the condition $\Delta C^0 = 3.0$ mM and $\sigma_{ex} = 4.0$ mN/m. A single GUV containing 98.0 mM sucrose solution was held at the tip of a micropipette using a tension on the bilayer of 4.0 mN/m in chamber A, containing 98.0 mM glucose solution, for 2 min; then, the GUV was transferred into chamber B, containing 95.0 mM glucose solution. The projection length, ΔL, of the GUV inside the micropipette decreased with time to an equilibrium value, ΔL_{eq}, which remained constant for a long time, then suddenly the GUV was aspirated

into the micropipette (i.e., pore formation occurred). Using Eq. 2, we obtained the $\Delta V/V_0$ ratio of the GUV, which was converted into $\Delta r/r_0$ using $\Delta V/V_0 \approx 3(\Delta r/r_0)$. Fig. 4 *A* shows the time course of $\Delta r/r_0$ for several GUVs subjected to the same conditions. $\Delta r/r_0$ increased with time to reach an equilibrium value, $\Delta r_{eq}/r_0$, which remained constant for a long time, until sudden rupture occurred. The values of $\Delta r_{eq}/r_0$ were similar for all examined GUVs (i.e., $\Delta r_{eq}/r_0 = (8.6 \pm 0.2) \times 10^{-3}$ (n =17)).

The second experiment used the condition $\Delta C^0 = 4.0$ mM and $\sigma_{ex} = 5.0$ mN/m, which produces a larger membrane tension. Fig. 4 *B* shows the time course of $\Delta r/r_0$ of several GUVs under the same conditions. After transfer of the GUV into chamber B, $\Delta r/r_0$ increased with time and the GUV was aspirated into the micropipette at various values of $\Delta r/r_0$ (0.0043–0.010) before reaching a constant value of $\Delta r/r_0$ (i.e., the swelling equilibrium) for most GUVs. The rupture of the GUVs occurred stochastically, and the membrane tensions at the time of rupture were different.

Two different time courses of volume change (or radius change) of GUVs were observed in Π-induced pore formation (Fig. 4, *A* and *B*). In these experiments, there are two sources of membrane tension (σ_{ex} and σ_{osm}^{eq}); consequently,

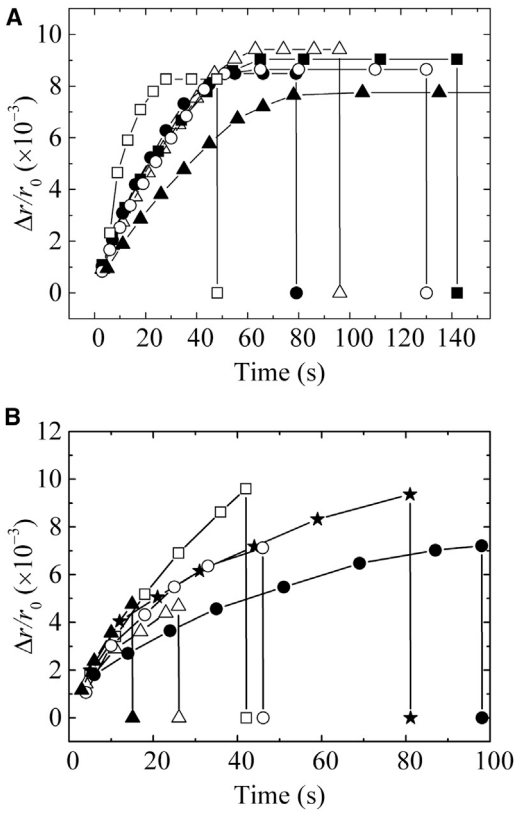

FIGURE 4 The time courses of the fractional change of radius of a GUV, $\Delta r/r_0$, under Π and σ_{ex}. The curves represent the $\Delta r/r_0$ results for several GUVs for (*A*) $\Delta C^0 = 3.0$ mM and $\sigma_{ex} = 4.0$ mN/m and (*B*) $\Delta C^0 = 4.0$ mM and $\sigma_{ex} = 5.0$ mN/m.

$\sigma_t = \sigma_{ex} + \sigma_{osm}^{eq}$. For relatively small σ_t, the radius of the GUV increased to an equilibrium value, r_{eq}, which remained constant for a long time, indicating that σ_t also remained constant for a long time after the swelling equilibrium, and then suddenly the GUV ruptured (Fig. 4 *A*). If we observe many GUVs under the same conditions, it is clear that the rupture of GUVs occurred stochastically (Fig. 4 *A*). These experimental results are different from the theoretical predictions of the effect of Π on the radius (or volume) of vesicles (i.e., immediately after the radius of a vesicle reaches a critical value, pore formation in the vesicle membrane occurs and the vesicle radius rapidly decreases) (6,14), but are very similar to the phenomenon observed in the σ_{ex}-induced rupture of a GUV (27–29). The mean value of $(\sigma_{osm}^{eq})^{ex}$ obtained experimentally by Eq. 7 and $\Delta r_{eq}/r_0 = (8.6 \pm 0.2) \times 10^{-3}$ was 4.1 ± 0.1 mN/m, and therefore, $\sigma_t = \sigma_{ex} + \sigma_{osm}^{eq} = 8.1$ mN/m. Furthermore, $(\sigma_{osm}^{eq})^{th} = 4.3 \pm 0.7$ mN/m (Table S5), which agrees with the experimental value. In contrast, for relatively large σ_t, as shown in Fig. 4 *B*, the radius of a GUV increased with time and the rupture of the GUV occurred at various values of $\Delta r/r_0$ (0.0043−0.010) before reaching the swelling equilibrium. In this case ($\overline{r_0} = 15.7$ μm), $(\sigma_{osm}^{eq})^{th} = 5.8$ mN/m, and hence, the theoretical value of $\sigma_t = \sigma_{ex} + \sigma_{osm}^{eq}$ is 5.0 + 5.8 = 10.8 mN/m at swelling equilibrium, which is much larger than the σ_{ex} values in the σ_{ex}-induced rupture of DOPC-GUVs (27). Therefore, rupture occurred before the membrane tension of a GUV reached equilibrium. In this situation, the membrane tension increased with time because the radius of the GUV increased with time and then pore formation occurred suddenly. Membrane tension at the time of rupture of the GUV varied widely, similar to tension-induced rupture when tension changed with time (25,26).

General discussion

The analysis of the effect of Π on the σ_{ex}-induced rupture of a DOPC-GUV (Fig. 1) provided the values of the membrane tension due to Π, σ_{osm}^{eq}. If $\sigma_{osm}^{eq} \geq 6.0$ mN/m, pore formation occurred in the GUV membrane (Fig. 3 *C*). It is generally considered that thermal fluctuation in the lateral density of a lipid membrane induces a prepore (27). According to the classical theory of tension-induced pore formation (36–38), once a prepore with radius r_p is formed in the membrane, the total free energy of the system changes by an additional free-energy component (called the free energy of a prepore, $U(r_p, \sigma_t)$) consisting of two terms: one term ($-\pi r_p^2 \sigma_t$) is associated with lateral tension (σ_t) and favors expansion of the prepore, and the other term ($2\pi r_p \Gamma$) is associated with the line tension (Γ) of the prepore edge and favors prepore closure. The free energy of a prepore, $U(r_p, \sigma_t)$, can therefore be expressed as

$$U(r_p, \sigma_t) = 2\pi r_p \Gamma - \pi r_p^2 \sigma_t. \quad (10)$$

U (r_p, σ_t) has a maximum of $U_a = U$ (r_p*) $= \pi\Gamma^2/\sigma_t$ at $r = r_p$* ($= \Gamma/\sigma_t$) (Fig. 5). If the radius of a prepore is less than the critical radius, r_p*, it closes quickly. However, if the radius expands and reaches r_p*, the prepore transforms into a pore. In the case of σ_{ex}-induced rupture, the radius of a prepore reaches r_p* stochastically and hence, rupture occurs stochastically. Experimentally, the decrease in the fraction of intact GUVs fits a single-exponential decay function, indicating that the rupture can be considered as an irreversible two-state transition (27–29). This fitting also provided the rate constant of σ_{ex}-induced pore formation, which increased with an increase in σ_{ex} (26–28). Recently, the values of the activation energy of σ_{ex}-induced pore formations were experimentally determined, and the analysis of the activation energy clearly indicated that the dependence of U_a on σ_{ex} in the classical theory is correct (29,39). On the basis of this theory, we consider the Π-induced pore formation in a GUV, where $\sigma^{eq}_{osm} = \sigma_t$. At $\Delta C^0 \leq 3.7$ mM (i. e., $\sigma^{eq}_{osm} \leq 5.3$ mN/m) (Table S4), the corresponding membrane tensions are so small that the activation energy is much higher than the thermal energy. At $\Delta C^0 \geq 4.2$ mM (i, e., $\sigma^{eq}_{osm} \geq 6.0$ mN/m), the corresponding membrane tension increases and therefore the activation energy becomes sufficiently low to induce pore formation.

Here, we consider whether σ^{eq}_{osm} and σ_{ex} have the same effect on vesicle membranes as lateral tension on the membrane. For the experiments shown in Fig. 1, both σ_{ex} and σ^{eq}_{osm} were applied to a GUV, and hence the total tension on the GUV membrane was $\sigma_t (= \sigma_{ex} + \sigma^{eq}_{osm})$. For these experiments, we can also use one measure of the rate of σ_t-induced rupture of GUVs, namely, the fraction of ruptured GUVs among all examined GUVs at 6 min, P_{pore} (360 s) (Tables S6 and S7). We consider that leakage of sucrose occurs when pore formation occurs in the GUV membrane, and therefore, P_{pore} (360 s) $= P_{Leak}$ (360 s). The theoretical values of σ_t for each condition of the experiments depicted in Fig. 1 were determined (Tables S6 and S7) and the relationship between P_{pore} (360 s) versus σ_t was plotted in Fig. 3 *C* (*solid circles*). If we compare the values of $\sigma_t = \sigma^{eq}_{osm}$ (*open squares*) and those of $\sigma_t = \sigma_{ex} + \sigma^{eq}_{osm}$ ($\sigma_{ex} = 3.3 - 5.5$ mN/m) (*solid circles*), both agree with each other within the limits of experimental errors. Therefore, we can conclude that P_{pore} (360 s) is mainly determined by σ_t, irrespective of the contribution of σ_{ex}. On the other hand, the results of the σ_{ex}-induced rupture of a DOPC-GUV show that at $\sigma_{ex} = 7.0$ mN/m, the rate constant of pore formation, k_p, was $(3.1 \pm 0.4) \times 10^{-3}$ s^{-1} (Fig. 1 *C*, *open squares*) (27), P_{pore} (360 s) $= 0.55 \pm 0.02$, and at $\sigma_{ex} \geq 7.0$ mN/m, k_p increased with σ_{ex}. The agreement of P_{Leak} (360 s) (Fig. 3 *C*) with P_{pore} (360 s) at $\sigma_t = 7.0$ mN/m, and the similarity of the dependence of the rate of pore formation (judging from P_{Leak} (360 s) and k_p) on membrane tension (σ^{eq}_{osm} or σ_{ex}), indicate that σ^{eq}_{osm} is equivalent to σ_{ex}, supporting the conclusion that P_{pore} (360 s) is mainly determined by σ_t, irrespective of the contribution of σ_{ex}. These results indicate that both σ^{eq}_{osm} and σ_{ex} contribute to the total tension equivalently (i.e., $\sigma_t = \sigma_{ex} + \sigma^{eq}_{osm}$) and induce pore formation in the GUV membrane, i.e., σ^{eq}_{osm} cannot be distinguished from σ_{ex}. Based on this conclusion, we can reasonably consider that σ_{ex} can induce leakage of sucrose due to pore formation in the GUV membrane in a manner similar to σ^{eq}_{osm}-induced leakage, although this could not be observed directly in the experiments presented here due to the rapid aspiration of the GUVs (27–29).

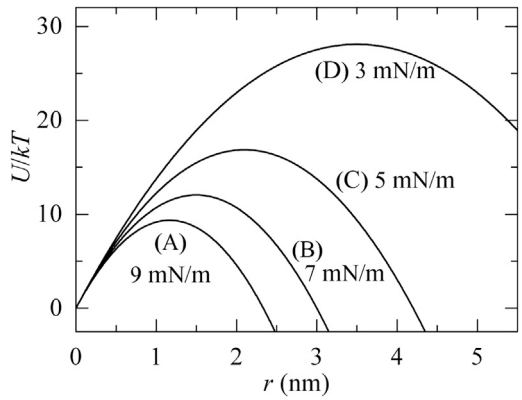

FIGURE 5 Dependence of the free-energy profile of a prepore in a DOPC-GUV on its radius for various tensions due to Π, σ^{eq}_{osm}: (*A*) 9.0, (*B*) 7.0, (*C*) 5.0, and (*D*) 3.0 mN/m. $U(r)$ is calculated according to Eq. 10 using $\Gamma = 10.5$ pN.

If the radius of a prepore reaches r_p* during the thermal fluctuation of the membrane, a pore is formed, inducing a rapid leakage of internal sucrose solution due to the Laplace pressure. This induces a rapid decrease in GUV volume (Fig. 3 *A*), and therefore, the tension due to stretching of the membrane disappears. Subsequently, the pore rapidly closes due to the line tension of the pore. Generally, the dynamics of closing of a large pore induced by tension have been investigated experimentally (16,24,40,41), and the theories of the evolution of a pore induced by tension can explain well the results of closing of large pores (42,43). Therefore, we can reasonably consider that the evolution of the Π-induced pore can be explained by these theories, although we did not get any quantitative information on the closing of the Π-induced pore in this report. During the decrease in GUV volume due to the efflux of sucrose solution, a submicroscopic daughter vesicle may be formed and subsequently released from the parent GUV, which cannot be observed by phase-contrast microscopy (22,44). In this case, the area of the GUV also decreases. After the pore closes, the concentration of sucrose inside the GUV is still higher than that of glucose outside the GUV, and hence the GUV swells again. When the GUV reswelled to a large enough volume to produce a large membrane tension, the second rapid leakage of sucrose occurred (Fig. S3). It is noted that the phase contrast of the resealed GUVs was similar to that of the intact GUVs, because the

amount of sucrose leakage was small. Therefore, it is difficult to distinguish intact GUVs from resealed GUVs after Π-induced pore formation.

It is noteworthy to consider the dependence of Π-induced tension, σ_{osm}^{eq}, on the radius of the vesicles. If the values of the parameters other than the radius are the same, according to Eq. 4, σ_{osm}^{eq} is proportional to the radius of the vesicles when ΔC^{eq} is the same. For example, σ_{osm}^{eq} for GUVs with a radius of 10 μm is 100 times larger than σ_{osm}^{eq} for LUVs with a radius of 100 nm. However, for GUVs, ΔC^{eq} is much smaller than that ΔC^0, in contrast to LUVs, where $\Delta C^{eq} \approx \Delta C^0$. For example, at $C_{in}{}^0 = 98.0$ mM and $C_{out} = 96.0$ mM (hence $\Delta C^0 = 2.0$ mM), ΔC^{eq} for GUVs with a radius of 10 μm is 0.2 mM, but ΔC^{eq} for LUVs with a radius of 100 nm is 1.9 mM (as estimated theoretically using Eqs. 5 and 7). The final size dependence of σ_{osm}^{eq} is determined by $\Delta r_{eq}/r_0$ according to Eq. 7. Under the above concentration conditions, $\Delta r_{eq}/r_0$ for GUVs with a radius of 10 μm is 6.2×10^{-3}, which is 13 times larger than that for LUVs with a radius of 100 nm ($= 4.9 \times 10^{-4}$), and hence, σ_{osm}^{eq} for the GUV is 13 times larger than σ_{osm}^{eq} for the LUV. To validate this theory on the radius dependence of σ_{osm}^{eq}, we measured a change in a physical property of lipid membranes induced by Π. It was recently reported that the membrane stretching due to lateral tension increases the fluidity of lipid membranes (45,46) and the diffusion coefficient of lipid molecules (45–47). To monitor the fluidity of the membranes, we used generalized emission polarization value (GP) of Laurdan in membranes, because it is generally considered that with an increase in fluidity of lipid membranes the interaction of water molecules with a Laurdan molecule in the membrane interface increases, which causes the GP value to decrease (48,49). Both GP values for DOPC-LUVs and DOPC-GUVs decreased with an increase in ΔC^0, indicating that the fluidity of the membranes of both vesicles increased with Π, but to induce similar decrements of the GP values ~10 times higher ΔC^0 values were required for DOPC-LUVs compared with DOPC-GUVs (Fig. S4, *B* and *D*). These results suggest that the stretching of the membranes due to lateral tension increased with an increase in Π, but to induce similar amounts of stretching, ~10 times higher ΔC^0 values were required for DOPC-LUVs compared with DOPC-GUVs. After converting ΔC^0 to σ_{osm}^{eq}, we found that the GP values were essentially the same in DOPC-GUVs and DOPC-LUVs at the same σ_{osm}^{eq} (Fig. S4 *E*). This result supports the theory on the radius dependence of σ_{osm}^{eq}.

As described above in Results and Discussion, when GUVs are transferred to a hypotonic solution, the volume of the GUVs increases due to the osmotic pressure. In the initial response of the GUVs, we have to consider the hidden-excess area (23). Thermal undulation motion of GUV membranes (50,51) and long thin (submicron) tubular protrusions (52,53) can be considered as sources of the hidden-excess membrane area of the GUVs. To prevent the influence of the hidden-excess area, for the experiment using micropipettes (e.g., Figs. 1, 2, and 4), we first applied a small aspiration pressure on a GUV to provide a tension of 0.5 mN/m for 2 min to incorporate the hidden-excess area, which is similar to the method of (17,27). Based on (51), this is a sufficient condition to incorporate hidden-excess area.

Recently it was reported that sucrose or glucose may influence the bending modulus of lipid membranes, κ (54–57). Some data indicate that the bending modulus decreased with sucrose (or glucose) concentration, and other data indicate no effects. Moreover, its mechanism is not clear yet. On the other hand, the bending modulus is related to the elastic modulus of the bilayer of the GUV, K_{bil}, and the bilayer thickness, d (e.g., $\kappa \propto K_{bil}d^2$) (58). Hence, the value of K_{bil} may depend on sucrose (or glucose) concentration if the value of d does not depend on sucrose (or glucose) concentration. We measured the values of K_{bil} of DOPC-GUV in various sucrose/glucose concentrations from 50 to 200 mM and found that they were almost the same in this limited range of sucrose/glucose concentration (Fig. S2 *B*). In all experiments in this report, we used 78.0−98.0 mM sucrose/glucose, and hence we can consider that the effect of sucrose/glucose concentration on their results was negligible.

The above results clearly show that GUVs, which are cell-sized vesicles, are weak against Π. Pore formation in the plasma membrane of cells causes cell death, yet solute concentrations outside of cells can change easily. To prevent Π-induced cell death, cells have had to modify their membrane structure by incorporating cholesterol (34) and mechanosensitive channels (2) into their plasma membranes during the evolution of life. It is well known that cholesterol increases the line tension of pores or prepores and therefore the probability of pore formation in lipid membranes decreases (24,25,41), and also that mechanosensitive channels open when membranes are stretched by Π (3,4). Therefore, cells are much stronger against Π than GUVs of lipid membranes lacking cholesterol.

CONCLUSIONS

In this report, we succeeded in determining the membrane tension, σ_{osm}^{eq}, of DOPC-GUVs under osmotic pressure (Π) experimentally for the first time, to the best of our knowledge, by analyzing the effects of Π on the constant tension-induced rupture of GUVs. We also estimated σ_{osm}^{eq} by analysis of the volume change of the GUVs under small Π. These experimentally estimated values of σ_{osm}^{eq} agreed with their theoretical values within the limits of their experimental errors. The total tension due to σ_{osm}^{eq} and the external tension determine the response of GUVs: at lower total tensions, the radius of the GUVs increased to an equilibrium value, r_{eq}, which remained constant for a long time, and then stochastic rupture of the GUV occurred, as is the case

for the constant-tension-induced rupture of GUVs. These results provide quantitative information on membrane tension due to Π, which is valuable for research on the effects of Π on the activities of membrane proteins and membrane active peptides.

SUPPORTING MATERIAL

Supporting Materials and Methods, four figures, and seven tables are available at http://www.biophysj.org/biophysj/supplemental/S0006-3495(16)30877-3.

AUTHOR CONTRIBUTIONS

S.U.A.S. and M.Y. designed the research. S.U.A.S., C.G., and M.M. performed the experiments. S.U.A.S., C.G., M.A.S.K., and M.Y. analyzed data. S.U.A.S., C.G., and M.Y. wrote the article.

ACKNOWLEDGMENTS

This work was supported in part by a Grant-in-Aid for Scientific Research (B) (No. 15H04361) from the Japan Society for the Promotion of Science to M.Y. Part of this research was carried out under the Cooperative Research Projectof the Research Institute of Electronics, Shizuoka University.

REFERENCES

1. N. Sperelakis, editor 2012. Cell Physiology Source Book, 4th ed. Essentials of membrane biophysics. Academic press, London.
2. Sachs, F. 2010. Stretch-activated ion channels: what are they? *Physiology (Bethesda).* 25:50–56.
3. Sukharev, S. I., P. Blount, …, C. Kung. 1994. A large-conductance mechanosensitive channel in *E. coli* encoded by mscL alone. *Nature.* 368:265–268.
4. Levina, N., S. Tötemeyer, …, I. R. Booth. 1999. Protection of *Escherichia coli* cells against extreme turgor by activation of MscS and MscL mechanosensitive channels: identification of genes required for MscS activity. *EMBO J.* 18:1730–1737.
5. Taupin, C., M. Dvolaitzky, and C. Sauterey. 1975. Osmotic pressure induced pores in phospholipid vesicles. *Biochemistry.* 14:4771–4775.
6. Koslov, M. M., and V. S. Markin. 1984. A theory of osmotic lysis of lipid vesicles. *J. Theor. Biol.* 109:17–39.
7. Sun, S. T., A. Milon, …, Y. Nakatani. 1986. Osmotic swelling of unilamellar vesicles by the stopped-flow light scattering method. Elastic properties of vesicles. *Biochim. Biophys. Acta.* 860:525–530.
8. Li, W., T. S. Aurora, …, H. Z. Cummins. 1986. Elasticity of synthetic phospholipid vesicles and submitochondrial particles during osmotic swelling. *Biochemistry.* 25:8220–8229.
9. Rutkowski, C. A., L. M. Williams, …, H. Z. Cummins. 1991. The elasticity of synthetic phospholipid vesicles obtained by photon correlation spectroscopy. *Biochemistry.* 30:5688–5696.
10. Ertel, A., A. G. Marangoni, …, J. M. Wood. 1993. Mechanical properties of vesicles. I. Coordinated analysis of osmotic swelling and lysis. *Biophys. J.* 64:426–434.
11. Hallett, F. R., J. Marsh, …, J. M. Wood. 1993. Mechanical properties of vesicles. II. A model for osmotic swelling and lysis. *Biophys. J.* 64:435–442.
12. Mui, B. L.-S., P. R. Cullis, …, T. D. Madden. 1993. Osmotic properties of large unilamellar vesicles prepared by extrusion. *Biophys. J.* 64:443–453.
13. Levin, Y., and M. A. Idiart. 2004. Pore dynamics of osmotically stressed vesicles. *Physica A.* 331:571–578.
14. Idiart, M. A., and Y. Levin. 2004. Rupture of a liposomal vesicle. *Phys. Rev. E Stat. Nonlin. Soft Matter Phys.* 69:061922.
15. Yamazaki, M. 2008. The single GUV method to reveal elementary processes of leakage of internal contents from liposomes induced by antimicrobial substances. *Adv. Planar Lipid Bilayers and Liposomes.* 7:121–142.
16. Sandre, O., L. Moreaux, and F. Brochard-Wyart. 1999. Dynamics of transient pores in stretched vesicles. *Proc. Natl. Acad. Sci. USA.* 96:10591–10596.
17. Rawicz, W., K. C. Olbrich, …, E. Evans. 2000. Effect of chain length and unsaturation on elasticity of lipid bilayers. *Biophys. J.* 79:328–339.
18. Baumgart, T., S. T. Hess, and W. W. Webb. 2003. Imaging coexisting fluid domains in biomembrane models coupling curvature and line tension. *Nature.* 425:821–824.
19. Islam, M. Z., J. M. Alam, …, M. Yamazaki. 2014. The single GUV method for revealing the functions of antimicrobial, pore-forming toxin, and cell-penetrating peptides or proteins. *Phys. Chem. Chem. Phys.* 16:15752–15767.
20. Hotani, H. 1984. Transformation pathways of liposomes. *J. Mol. Biol.* 178:113–120.
21. Ho, J. C. S., P. Rangamani, …, A. N. Parikh. 2016. Mixing water, transducing energy, and shaping membranes: autonomously self-regulating giant vesicles. *Langmuir.* 32:2151–2163.
22. Boroske, E., M. Elwenspoek, and W. Helfrich. 1981. Osmotic shrinkage of giant egg-lecithin vesicles. *Biophys. J.* 34:95–109.
23. Olbrich, K., W. Rawicz, …, E. Evans. 2000. Water permeability and mechanical strength of polyunsaturated lipid bilayers. *Biophys. J.* 79:321–327.
24. Karatekin, E., O. Sandre, …, F. Brochard-Wyart. 2003. Cascades of transient pores in giant vesicles: line tension and transport. *Biophys. J.* 84:1734–1749.
25. Evans, E., V. Heinrich, …, W. Rawicz. 2003. Dynamic tension spectroscopy and strength of biomembranes. *Biophys. J.* 85:2342–2350.
26. Evans, E., and B. A. Smith. 2011. Kinetics of hole nucleation in biomembrane rupture. *New J. Phys.* 13:095010.
27. Levadny, V., T. A. Tsuboi, …, M. Yamazaki. 2013. Rate constant of tension-induced pore formation in lipid membranes. *Langmuir.* 29:3848–3852.
28. Karal, M. A. S., V. Levadnyy, …, M. Yamazaki. 2015. Electrostatic interaction effects on tension-induced pore formation in lipid membranes. *Phys. Rev. E Stat. Nonlin. Soft Matter Phys.* 92:012708.
29. Karal, M. A. S., and M. Yamazaki. 2015. Communication: activation energy of tension-induced pore formation in lipid membranes. *J. Chem. Phys.* 143:081103.
30. Yoshitani, T., and M. Yamazaki. 2008. Water permeability of lipid membranes of GUVs and its dependence on actin cytoskeletons inside the GUVs. *Proc. IEEE Int. Symp. Micro-NanoMechatronics and Human Sci.* 2008:130–134.
31. Grattoni, A., M. Merlo, and M. Ferrari. 2007. Osmotic pressure beyond concentration restrictions. *J. Phys. Chem. B.* 111:11770–11775.
32. Minkov, I., E. D. Manev, …, K. H. Kolikov. 2013. Equilibrium and dynamic behavior of aqueous solutions with varied concentration at constant and variable volume. *Sci. World J.* 2013:876897.
33. De Gennes, P.-G., F. Brochard-Wyart, and D. Quere. 2004. Capillarity and Wetting Phenomena; Drops, Bubbles, Pearls, Waves. Springer, New York.
34. Needham, D., and R. S. Nunn. 1990. Elastic deformation and failure of lipid bilayer membranes containing cholesterol. *Biophys. J.* 58:997–1009.
35. Karal, M. A. S., J. M. Alam, …, M. Yamazaki. 2015. Stretch-activated pore of the antimicrobial peptide, magainin 2. *Langmuir.* 31:3391–3401.

36. Deryagin, B. V., and Y. V. Gutop. 1962. Theory of the breakdown (rupture) of free films. *Kolloidn. Zh.* 24:370–374.
37. Litster, J. D. 1975. Stability of lipid bilayers and red blood cell membranes. *Phys. Lett. A.* 53:193–194.
38. Fuertes, G., D. Giménez, …, J. Salgado. 2011. A lipocentric view of peptide-induced pores. *Eur. Biophys. J.* 40:399–415.
39. Karal, M. A. S., V. Levadnyy, and M. Yamazaki. 2016. Analysis of constant tension-induced rupture of lipid membranes using activation energy. *Phys. Chem. Chem. Phys.* 18:13487–13495.
40. Srividya, N., S. Muralidharan, …, B. Tripp. 2008. Determination of the line tension of giant vesicles from pore-closing dynamics. *J. Phys. Chem. B.* 112:7147–7152.
41. Portet, T., and R. Dimova. 2010. A new method for measuring edge tensions and stability of lipid bilayers: effect of membrane composition. *Biophys. J.* 99:3264–3273.
42. Brochard-Wyart, F., P.-G. De Gennes, and O. Sandre. 2000. Transient pores in stretched vesicles: role of leak-out. *Physica A.* 278:32–51.
43. Ryham, R., I. Berezovik, and F. S. Cohen. 2011. Aqueous viscosity is the primary source of friction in lipidic pore dynamics. *Biophys. J.* 101:2929–2938.
44. Mavčič, B., B. Babnik, …, V. Kralj-Iglič. 2004. Shape transformation of giant phospholipid vesicles at high concentrations of $C_{12}E_8$. *Bioelectrochemistry.* 63:183–187.
45. Muddana, H. S., R. R. Gullapalli, …, P. J. Butler. 2011. Atomistic simulation of lipid and DiI dynamics in membrane bilayers under tension. *Phys. Chem. Chem. Phys.* 13:1368–1378.
46. Reddy, A. S., D. T. Warshaviak, and M. Chachisvilis. 2012. Effect of membrane tension on the physical properties of DOPC lipid bilayer membrane. *Biochim. Biophys. Acta.* 1818:2271–2281.
47. Butler, P. J., G. Norwich, …, S. Chien. 2001. Shear stress induces a time- and position-dependent increase in endothelial cell membrane fluidity. *Am. J. Physiol. Cell Physiol.* 280:C962–C969.
48. De Vequi-Suplicy, C. C., C. R. Benatti, and M. T. Lamy. 2006. Laurdan in fluid bilayers: position and structural sensitivity. *J. Fluoresc.* 16:431–439.
49. Lakowicz, J. R. 1999. Principles of Fluorescence Spectroscopy, 2nd ed. Kluwer Academic, Dordrecht, the Netherlands.
50. Evans, E., and W. Rawicz. 1990. Entropy-driven tension and bending elasticity in condensed-fluid membranes. *Phys. Rev. Lett.* 64:2094–2097.
51. Vitkova, V., J. Genova, and I. Bivas. 2004. Permeability and the hidden area of lipid bilayers. *Eur. Biophys. J.* 33:706–714.
52. Mathivet, L., S. Cribier, and P. F. Devaux. 1996. Shape change and physical properties of giant phospholipid vesicles prepared in the presence of an AC electric field. *Biophys. J.* 70:1112–1121.
53. Perutková, S., V. Kralj-Iglič, …, A. Iglič. 2010. Mechanical stability of membrane nanotubular protrusions influenced by attachment of flexible rod-like proteins. *J. Biomech.* 43:1612–1617.
54. Genova, J., A. Zheliaskova, and M. D. Mitov. 2006. The influence of sucrose on the elasticity of SOPC lipid membrane studied by the analysis of thermally induced shape fluctuation. *Colloids Surf. A Physicochem. Eng. Asp.* 282–283:420–422.
55. Shchelokovskyy, P., S. Tristram-Nagle, and R. Dimova. 2011. Effect of the HIV-1 fusion peptide on the mechanical properties and leaflet coupling of lipid bilayers. *New J. Phys.* 13:25004.
56. Drabik, D., M. Przybyło, …, M. Langner. 2016. The modified fluorescence based vesicle fluctuation spectroscopy technique for determination of lipid bilayer bending properties. *Biochim. Biophys. Acta.* 1858:244–252.
57. Nagle, J. F., M. S. Jablin, and S. Tristram-Nagle. 2016. Sugar does not affect the bending and tilt moduli of simple lipid bilayers. *Chem. Phys. Lipids.* 196:76–80.
58. Marsh, D. 1996. Lateral pressure in membranes. *Biochim. Biophys. Acta.* 1286:183–223.

Biophysical Journal, Volume *111*

Supplemental Information

Experimental Estimation of Membrane Tension Induced by Osmotic Pressure

Sayed Ul Alam Shibly, Chiranjib Ghatak, Mohammad Abu Sayem Karal, Md. Moniruzzaman, and Masahito Yamazaki

Supporting Material

Experimental Estimation of Membrane Tension Induced by Osmotic Pressure

Sayed Ul Alam Shibly,[a] Chiranjib Ghatak,[b] Mohammad Abu Sayem Karal,[a] Md. Moniruzzaman,[a] and Masahito Yamazaki[a,b,c,*]

[a] Integrated Bioscience Section, Graduate School of Science and Technology, Shizuoka University, Shizuoka, 422-8529, Japan, [b] Nanomaterials Research Division, Research Institute of Electronics, Shizuoka University, Shizuoka 422-8529, Japan, [c] Department of Physics, Faculty of Science, Shizuoka University, Shizuoka 422-8529, Japan.

S.1. Measurement of osmotic pressure of sucrose and glucose aqueous solution

The osmolality (mOsm/kg) of sucrose solution and glucose solution was measured by analyzing the freezing point depression of these solutions using Osmometer 3250 (Advanced Instrument Inc., Norwood, MA) at Japan Food Research Laboratories, Tama Institute (Tokyo, Japan). By correction of the volume change, we converted these osmolality (mOsm/kg) to the osmolarity (mOsm/L) (Table S1 & S2). Figure S1 shows the linear relationship between osmolarity (y) and molar concentration of sucrose (or glucose), C, when C is at and less than 98 mM, and the fitting equations for sucrose and glucose are $y = (1.03 \pm 0.01)\ C$ and $y = (1.04 \pm 0.02)\ C$, respectively. These results indicate that the ideal equation (van't Hoff's law) for Π can be used for these solutions within experimental errors, which agrees with the previous reports [1,2].

Figure S1

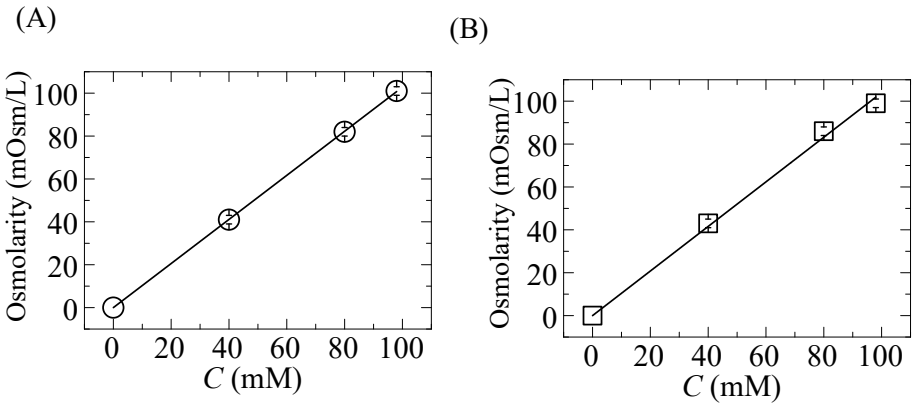

Figure S1**:** Osmotic pressure of sucrose and glucose aqueous solutions. Osmolarity (mOsmo/L) of sucrose solution (A), and glucose solution (B).

Table S1**:** Osmotic pressure of sucrose solution

C (mM)	Osmolality (mOsm/kg)	Osmolarity (mOsm/L)
98.0	104 ± 2	101 ± 2
80.0	84 ± 2	82 ± 2
40.0	42 ± 2	41 ± 2

Table S2**:** Osmotic pressure of glucose solution

C (mM)	Osmolality (mOsm/kg)	Osmolarity (mOsm/L)
98.0	101 ± 2	99 ± 2
80.0	88 ± 2	86 ± 2
40.0	44 ± 2	43 ± 2

Figure S2

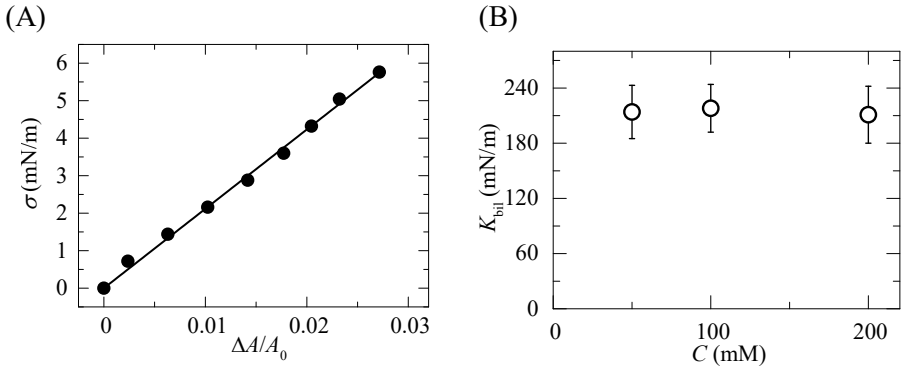

Figure S2**:** The elastic modulus of the bilayer of DOPC-GUV, K_{bil}. (A) Tension versus the fractional change in area of a DOPC-GUV in 100 mM sucrose (inside the GUV) / 100 mM glucose (outside the GUV). The slope of the line provided a K_{bil} value of 212 mN/m. (B) The elastic modulus of the bilayer of DOPC-GUV in various concentrations *C* of sucrose/glucose solutions. GUVs contained sucrose solution in their lumens, and in their outside glucose solution existed, and the concentrations of the sucrose solution and the glucose solution were the same.

Figure S3

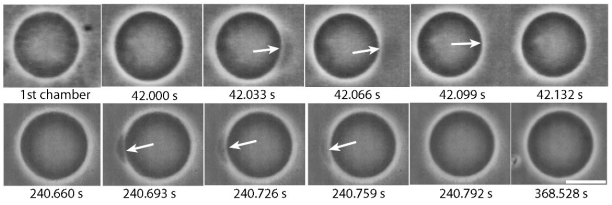

Figure S3**:** Behavior of DOPC-GUV under large Π. Phase-contrast microscopic images of a GUV after it was transferred into chamber B containing 78.0 mM glucose solution (i.e., ΔC^0 = 20.0 mM). The numbers below each image show the time in seconds after the transfer of the GUV into chamber B. The bar corresponds to 25 μm. The white arrows show two rapid, transient leakages of sucrose from DOPC-GUV upon Π.

Table S3: Comparison of $(\sigma_{osm}^{eq})^{ex}$ determined by the Π-induced volume change of GUVs with $(\sigma_{osm}^{eq})^{th}$: the analysis of the data in Figure 2

ΔC^0 (mM)	$\Delta V_{eq}/V_0$	$(\sigma_{osm}^{eq})^{ex}$ (mN/m)	$(\sigma_{osm}^{eq})^{th}$ (mN/m)	$\overline{r_0}$ (μm)
2.0	$(1.7 \pm 0.1) \times 10^{-2}$	2.7 ± 0.1	2.8 ± 0.7	14.5 ± 0.5
3.0	$(2.6 \pm 0.1) \times 10^{-2}$	4.1 ± 0.2	4.3 ± 0.7	16.2 ± 0.6

Table S4: The dependence of P_{Leak} (360 s) on $(\sigma_{osm}^{eq})^{th}$ (mN/m)

ΔC^o (mM)	$\overline{r_0}$ (μm)	$(\sigma_{osm}^{eq})^{th}$ (mN/m)	P_{Leak} (360 s)
1.0	13.0 ± 0.3	1.4	0.0
3.0	13.7 ± 0.4	4.2	0.09 ± 0.02
3.7	14.0 ± 0.3	5.3	0.12 ± 0.01
4.2	14.2 ± 0.3	6.0	0.31 ± 0.08
4.5	14.5 ± 0.5	6.5	0.53 ± 0.04
5.0	15.9 ± 0.5	7.3	0.84 ± 0.06
6.0	14.8 ± 0.5	8.9	0.98 ± 0.02
6.5	15.3 ± 0.5	9.7	1.0
8.0	14.2 ± 0.4	12.1	1.0

Table S5: Comparison of $(\sigma_{osm}^{eq})^{ex}$ determined by the Π-induced volume change of GUVs in the presence of external tension and $(\sigma_{osm}^{eq})^{th}$: the analysis of the data in Fig. 4A

ΔC^0 (mM)	σ_{ex} (mN/m)	$\Delta r_{eq}/r_0$	$(\sigma_{osm}^{eq})^{ex}$ (mN/m)	$(\sigma_{osm}^{eq})^{th}$ (mN/m)	$\overline{r_0}$ (μm)
3.0	4.0	$(8.6 \pm 0.2) \times 10^{-3}$	4.1 ± 0.1	4.3 ± 0.7	14.9 ± 0.6

Table S6: Fraction of ruptured GUVs, P_{pore} (360 s), in the results depicted in Figure 1. $\sigma_t = \sigma_{ex} + \sigma_{osm}^{eq}$
(A) ΔC^0 = 1.9 mM

σ_{ex} (mN/m)	$\overline{r_0}$ (μm)	$(\sigma_{osm}^{eq})^{th}$ (mN/m)	P_{pore} (360 s)	σ_t (mN/m)
4.5	12.5 ± 0.3	2.6	0.58 ± 0.06	7.1
5.0	14.4 ± 0.5	2.6	0.91 ± 0.02	7.6
5.5	13.4 ± 0.3	2.6	0.97 ± 0.02	8.1

Table S7: Fraction of ruptured GUVs, P_{pore} (360 s), in the results depicted in Figure 1. $\sigma_t = \sigma_{ex} + \sigma_{osm}^{eq}$
(B) ΔC^0 = 2.8 mM

σ_{ex} (mN/m)	$\overline{r_0}$ (μm)	$(\sigma_{osm}^{eq})^{th}$ (mN/m)	P_{pore} (360 s)	σ_t (mN/m)
3.3	13.6 ± 0.6	3.9	0.69 ± 0.06	7.2
3.8	13.7 ± 0.3	3.9	0.90 ± 0.02	7.7
4.3	13.8 ± 0.4	3.9	0.99 ± 0.02	8.2

S.2. The sources of the error of the experimental values of $\sigma_{\mathrm{osm}}^{\mathrm{eq}}$

It is necessary to consider the sources of the error of the experimental values of $\sigma_{\mathrm{osm}}^{\mathrm{eq}}$. One possibility is due to permeabilization of sucrose and glucose through DOPC membranes under the experimental conditions. It is reported that the membrane permeability coefficient of glucose, P, through dimiristoylphosphatidylcholine (DMPC) membrane in the liquid-crystalline phase in unilamellar vesicles is 1.5×10^{-12} m/s [3]. In the case of 100 mM and 0 mM glucose in the outside and in the inside of a GUV, respectively (i.e., $C_{\mathrm{out}}^{\mathrm{glu}} = 100$ mM, $C_{\mathrm{in}}^{\mathrm{glu}} = 0$ mM, and the concentration difference of glucose between the inside and the outside, $\Delta C_{\mathrm{glucose}}$, is 100 mM), the flux of glucose from the outside to the inside of the GUV (i.e., influx), J, is $J = P\Delta C_{\mathrm{glucose}} = 1.5 \times 10^{-10}$ mol/s·m^2. Therefore, the maximum rate of the increase in glucose concentration inside the GUV is as follows,

$$\frac{dC_{\mathrm{in}}^{\mathrm{glu}}}{dt} = \frac{1}{V_0} 4\pi r_0^2 J = \frac{3J}{r_0} = 4.5 \times 10^{-5} \quad [\mathrm{mM/s}] \tag{S1}$$

According to eq. S1, the maximum increase in C_{in} during 1800 s (= 30 min) is 0.08 mM, which is less than 5 % of ΔC^0. However, we also consider the permeabilization of sucrose from the inside to the outside of a GUV (i.e., efflux). There is no report to determine the accurate value of P of sucrose of PC membranes in vesicles. If we assume that P of sucrose is the same as that of glucose, we obtain the maximum rate of the decrease in sucrose concentration inside the GUV is 0.08 mM for 30 min, which is cancelled out by the increase in the glucose concentration inside the GUV, and therefore, ΔC^{eq} does not change. However, if the P values are different, ΔC^{eq} changes with time and concomitantly Π changes with time. It is reported that if the P value of substance A outside a GUV is different from that of substance B inside the GUV the diameter of the GUV changes with time [4]. In the control experiment of Fig. 2B (i.e., $\Delta C^0 = 0.0$ mM), we did not observe a significant change in $\Delta V/V_0$ for 20 min after the transfer of the GUV to chamber B. This indicates that the change of ΔC^{eq} due to the difference of the P value of sucrose and glucose is negligible for 20 min.

Another possibility is the increase in the glucose concentration outside the GUV due to the evaporation of water, which would decrease the volume of a GUV and therefore decreases the effects of Π. However, the control experiment of Fig. 2B indicates that the effect of water evaporation is negligible for 30 min (in this control experiment we kept GUVs in chamber A for 10 min and then in the chamber B for 20 min, and hence

we checked the water evaporation during 30 min). As described in the Materials and Methods, we made all the experiments for less than 30 min after we transferred a glucose solution and a GUV suspension to chamber A. Therefore, we consider that the water evaporation effect was negligible in our experiments.

The other possibility is due to the experimental method. In the chamber transfer method, we used a glass capillary with 1 mm diameter containing the same solution of chamber A. After a GUV was transferred into chamber B, the solution inside the capillary can be mixed inside chamber B, which could increase the osmolarity of the solution in chamber B. This would decrease the effective values of Π in the chamber transfer experiments shown in Figs. 2, 3, and 4.

S.3. Effect of Π on the GP values of Laurdan in DOPC-GUVs and DOPC-LUVs

As described in the main text, the transfer of DOPC-GUVs into a hypotonic solution resulted in Π-induced increase in the volume of the GUVs, which increased the area of the GUV membranes (i.e., the stretching of the membrane occurred). This may induce a change in fluidity of the GUV membranes, because it is recently reported that the membrane stretching due to lateral tension increases the fluidity of lipid membranes [5,6] and diffusion coefficient of lipid molecules [5-7]. To monitor such changes, we used a highly environment sensitive amphiphilic fluorophore, Laurdan, whose hydrocarbon chain incorporates into the membrane hydrophobic core while the fluorescing group locates at the region of the glycerols of the phospholipid in the membrane interface. Mechanistically, dipole-dipole interactions and reorientation of water molecules in the membrane interface due to changes in the fluidity and the hydrocarbon packing of lipid membranes cause spectral shifts in the Laurdan fluorescence that can be described by a generalized emission polarization value (GP) [8-10]. It was previously reported that the GP value of Laurdan in LUVs changes when osmotic pressure was applied [11].

S.3.1. Experimental methods

GUVs of DOPC/Laurdan mixture (molar ratio; 40:1) were prepared in water (MilliQ) containing 98.0 mM sucrose by natural swelling method of dry DOPC/Laurdan films described in Section 2.1. To obtain a purified GUV suspension, smaller vesicles and free Laurdan were removed using the membrane filtering method [12]. Firstly, the suspension was centrifuged (13000g, 20 min, 20 °C); the resulting supernatant was filtered through a Nuclepore membrane with 10-μm diameter pores (Whatman, GE Healthcare, UK, Ltd.,

Buckinghamshire, UK) in 98.0 mM sucrose for 1.0 h at a flow rate of 1.0 mL/min at room temperature (20–25 °C); the retained suspension (i.e., that which did not pass through the filter) was collected and used as the purified GUV suspension. Large Unilamellar Vesicles (LUVs) of DOPC/Laurdan mixture (molar ratio; 200:1) were prepared by the extrusion method [13,14]. An appropriate amount of phospholipid was first dissolved in chloroform containing the fluorescence probe Laurdan and the solvent was dried under N_2 gas and kept overnight under vacuum connected with a rotary pump. The lipid film was then hydrated by addition of 100.0 mM sucrose solution and extensively vortexed to form multilamellar vesicles (MLVs) of DOPC. Then the MLV suspension was subjected to freeze–thaw cycles (5 cycles) in liquid N_2 for 1.0 min, followed by warming to room temperature for 25–30 min. The resulting solution was extruded through a 200 nm-pore-size Nuclepore membrane using LF-1 LiposoFast apparatus (Avestin, Ottawa, Canada) until the solution became transparent (almost twenty times pass). To remove free Laurdan molecules in aqueous solution, the LUV suspension was passed through a Sephadex G-75 column equilibrated with 100 mM sucrose solution and the purified LUV suspension was obtained from fractions at the void volume [15].

A Hitachi F7000 spectrofluorometer (Hitachi, Tokyo, Japan) was used for fluorescence measurement. Fluorescence intensities of samples were measured at the excitation wavelength 350 nm, the emission wavelength range was 370-650 nm while both the excitation and emission band-pass were 5 nm. The temperature of the cell was held at 25 °C with a water bath circulator (Cool-Bit circulator, ACE-05AN, KELK Ltd., Tokyo, Japan). In case of LUV experiment, to induce osmotic pressure, we have performed the following method; we prepared five different solutions which have 100 mM sucrose in water as internal solution inside LUV and 90, 80, 70, 60, 50 mM sucrose in water as the external solutions. To induce osmotic pressure, in case of GUV experiments, we have taken certain amount of GUV containing solution (purified) which initially have 98.0 mM sucrose in water both as internal and external solution (osmotic pressure = 0) and then we gradually added water (MilliQ) to make the external solution hypotonic. The fluorescence intensity of the Laurdan in all these solutions were measured after certain incubation times (5 min) to attain the equilibrium. The correction of the fluorescence intensity due to the dilution was done. The GP values of Laurdan in different liposomes were calculated using the following formula: $GP = (I_{439} - I_{483}) / (I_{439} + I_{483})$ where, I_{439} and I_{483} denotes fluorescence intensities at 439 nm and 483 nm, respectively. In this context, it is important to understand that these measurements do not relate to emission polarization but polarization of the

fluorophore itself. In other words, GP does not relate to fluorescence emission polarization but instead to the electric polarization of the fluorophore due to the solvent environment. The lipid concentrations in the GUV suspensions and the LUV suspensions for fluorescence measurements were 14 μM and 180 μM, respectively, which were determined by the Bartlett method [16].

S.3.2. Effect of Π on the GP values of Laurdan in DOPC-GUVs and DOPC-LUVs

Figure S4A shows normalized fluorescence emission spectra of Laurdan in DOPC-GUVs under Π due to ΔC^0. All the spectra show a peak at 483 nm and a pronounced shoulder-like feature around 439 nm. These results revealed that an increase in ΔC^0 caused a decrease in the intensity around the 439 nm shoulder region. In a control experiment in which the GUV suspension was diluted with 98.0 mM sucrose solution, the normalized spectra did not change. Figure S4B shows that the GP values decreased from −0.156 to −0.203 with an increase in ΔC^0 from 0 to 4.0 mM. It is generally considered that with an increase in fluidity of lipid membranes the interaction of water molecules with a Laurdan molecule in the membrane interface increases, which decreases the GP value [8-10]. On the other hand, it is recently reported that the membrane stretching due to lateral tension increases the fluidity of lipid membranes [5,6] and diffusion coefficient of lipid molecules [5-7]. Therefore, the results shown in Fig. S4B suggest that the stretching of the DOPC membrane increases with ΔC^0. For comparison, we investigated the effect of Π on the GP values of Laurdan in DOPC-LUVs with a mean diameter of 200 nm. Figure S4C shows the fluorescence emission spectra of Laurdan in these DOPC-LUVs containing 100.0 mM sucrose solution under Π due to different ΔC^0, and Figure S4D shows that the GP values of Laurdan in these DOPC-LUVs decreased from −0.158 to −0.209 with an increase in ΔC^0 from 0 to 50 mM. Inducing the same decrease in GP values required ~10 times higher ΔC^0 for DOPC-LUVs compared with DOPC-GUVs. By conversion of ΔC^0 into $\sigma_{\mathrm{osm}}^{\mathrm{eq}}$ using the average values of the radius (10 μm for the GUVs and 0.10 μm for the LUVs), we obtained the dependences of the GP values on $\sigma_{\mathrm{osm}}^{\mathrm{eq}}$ for DOPC-GUVs and DOPC-LUVs (Figure S4E). The GP values at the same $\sigma_{\mathrm{osm}}^{\mathrm{eq}}$ were essentially same in DOPC-GUVs and DOPC-LUVs, and the GP values gradually decreased with an increase in $\sigma_{\mathrm{osm}}^{\mathrm{eq}}$.

Figure 3B shows that the probability of leakage, P_{Leak} (360 s), for DOPC-GUVs was almost 0 at $\Delta C^0 \leq$ 3.7 mM and increased with ΔC^0 at $\Delta C^0 \geq 4.2$ mM. This result indicates that $\sigma_{\mathrm{osm}}^{\mathrm{eq}}$ increases with ΔC^0 at $\Delta C^0 \leq 3.7$ mM, because no leakage of sucrose occurs. On the other hand, the GP value for the GUVs decreased with ΔC^0 at $\Delta C^0 \leq 4.0$ mM (Fig. S4B). These results are consistent, because the stretching of the membrane monotonously increases with $\sigma_{\mathrm{osm}}^{\mathrm{eq}}$ at $\Delta C^0 \leq 4.0$ mM, which induces the monotonous decrease in the GP values.

Figure S4

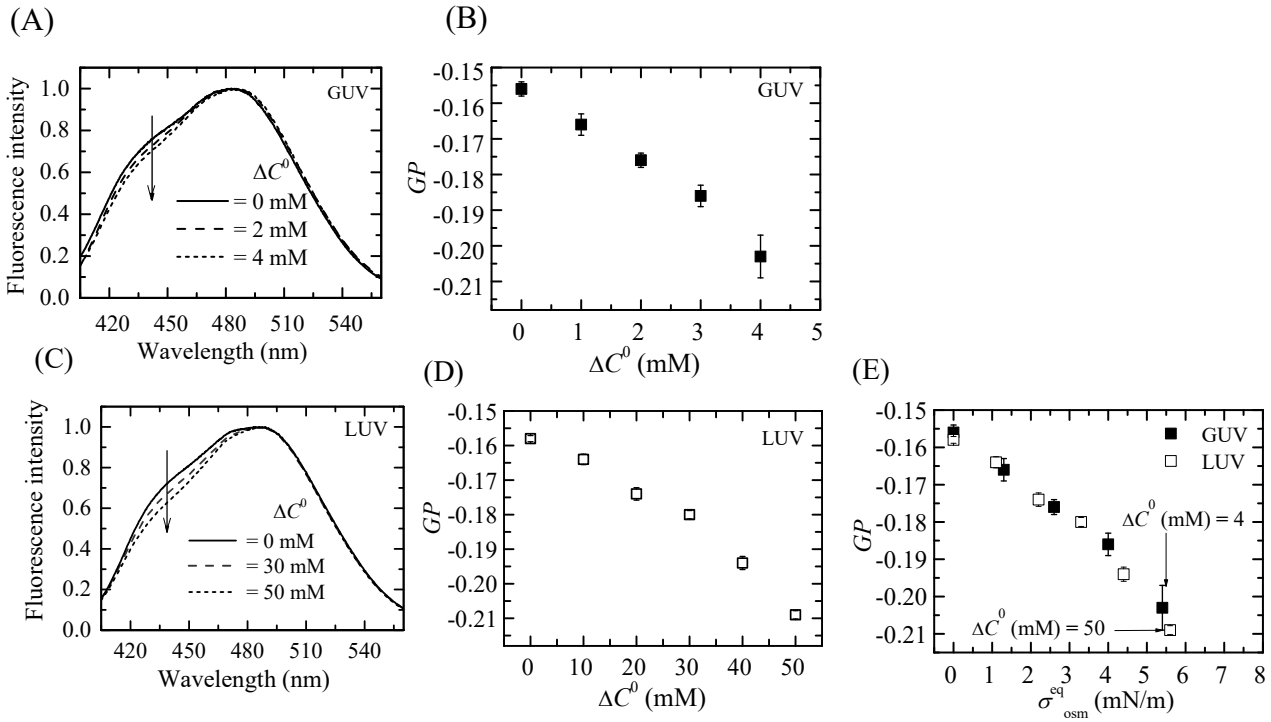

Figure S4**:** Effect of Π on GP values of Laurdan in DOPC-GUVs and DOPC-LUVs. Normalized fluorescence emission spectra of Laurdan in DOPC-GUVs (A) and DOPC-LUVs (C) in sucrose solution with different osmolarities. The GP values of Laurdan in DOPC-GUVs (B) and DOPC-LUVs (D) as a function of ΔC^0 at 25 °C. (E) Effect of $\sigma_{\mathrm{osm}}^{\mathrm{eq}}$ on the GP values of Laurdan in DOPC-LUVs (□) and GUVs (■) at 25 ˚C. (B) (D) (E) Mean GP values of three independent experiments were plotted.

Supporting References

(1) Grattoni, A., Merlo, M., and M. Ferrari. 2007. Osmotic pressure beyond concentration restrictions. J. Phys. Chem. B, 111:11770-11775.

(2) Minkov, I., Manev, E. D., Sazdanova, S. V., and K. H. Kolikov. 2013. Equilibrium and dynamic behavior of aqueous solutions with varied concentration at constant and variable volume. Sci. World J. 876897.

(3) Bresseleers, G. J. M., Goderis, H. L., and P. P. Tobback. 1984. Measurement of the glucose permeation rate across phospholipid bilayers using small unilamellar vesicles. Effect of membrane composition and temperature. Biochim. Biophys. Acta, 772:374-382.

(4) Pererlin, P., Arrigler, V., Diamant, H., and E. Haleva. 2012. Permeability of phospholipid membrane for small polar molecules determined from osmotic swelling of giant phospholipid vesicles. Adv. Planar Lipid Bilayers and Liposomes, 16:301-335.

(5) Muddana, H. S., Gullapalli, R. R., Manias, E., and P. J. Butler. 2011. Atomistic simulation of lipid and DiI dynamics in membrane bilayers under tension. Phys. Chem. Chem. Phys. 13, 1368-1378

(6) Reddy, A. S., Warshaviak, D. T., and M. Chachisvillis. 2012. Effect of membrane tension on the physical properties of DOPC lipid bilayer membrane. Biochim. Biophys. Acta, 1818, 2271-2281.

(7) Butler, P. J, Norwich, G., Weinbaum, S., and Chien, S. 2001. Shear stress induces a time- and position-dependent increase in endothelial cell membrane fluidity. Am. J. Physiol. Cell. Physiol. 280, C962-C969.

(8) Weber, G., and F. J. Farris. 1975. Synthesis and spectral properties of a hydrophobic fluorescent probe: 2-dimethylamino-6-propionyl naphthalene. Biochemistry, 18:3075-3078.

(9) De, Vequi-Suplicy C. C., Benatti, C. R., and M. T. Lamy. 2006. Laurdan in fluid bilayers: position and structural sensitivity. J. Fluoresc. 16:431-439.

(10) Lakowicz, J. R. 1999. Principles of fluorescence spectroscopy, 2nd Edition, Kluwer Academic Plenum Publishers, New York.

(11) Zhang, Y.-L., Frangos, J. A., and M. Chachisvilis. 2006. Laurdan fluorescence senses mechanical strain in the lipid bilayer membrane. Biochem. Biophys. Res. Comm. 347:838-841.

(12) Tamba, Y., Terashima, H., and M. Yamazaki. 2011. A membrane filtering method for the purification of giant unilamellar vesicles. Chem. Phys. Lipids, 164:351-358.

(13) Hope, M. J., Bally, M. B., Mayer, L. D., Janoff, A. S., and P. R. Cullis. 1986. Generation of multilamellar and unilamellar phospholipid vesicles. Chem. Phys. Lipids, 40:89–107.

(14) Mayer, L. D., Hope, M. J., and P. R. Cullis. 1986. Vesicles of variable sizes produced by a rapid extrusion procedure. Biochim. Biophys. Acta, 858:161–168.

(15) Tamba, Y., and M. Yamazaki. 2005. Single giant unilamellar vesicle method reveals effect of antimicrobial peptide magainin 2 on membrane permeability. Biochemistry, 44, 15823-15833.

(16) Bartlett, G. R. 1959. Phosphorous assay in column chromatography. J. Biol. Chem. 234:466–468.